Am J Cancer Res 2020;10(8):2480-2494
www.ajcr.us /ISSN:2156-6976/ajcr0109921

Original Article

Stabilization of oncogenic transcripts by the IGF2BP3/ELAVL1 complex promotes tumorigenicity in colorectal cancer

Kexin Li[1,2,3], Furong Huang[2], Yan Li[1,2,3], Dongdong Li[1,2,3], Hong Lin[1,2,3], Ruoxuan Ni[1,2,3], Qiao Zhang[1,2,3], Mei Zhao[1,2,3], Shengkai Huang[4], Liang Zou[5], Changzhi Huang[1,2,3]

[1]Department of Etiology and Carcinogenesis, National Cancer Center/National Clinical Research Center for Cancer/Cancer Hospital, Chinese Academy of Medical Sciences and Peking Union Medical College, Beijing 100021, China; [2]State Key Laboratory of Molecular Oncology, National Cancer Center/National Clinical Research Center for Cancer/Cancer Hospital, Chinese Academy of Medical Sciences and Peking Union Medical College, Beijing 100021, China; [3]Beijing Key Laboratory for Carcinogenesis and Cancer Prevention, National Cancer Center/National Clinical Research Center for Cancer/Cancer Hospital, Chinese Academy of Medical Sciences and Peking Union Medical College, Beijing 100021, China; [4]Department of Clinical Laboratory, National Cancer Center/National Clinical Research Center for Cancer/Cancer Hospital, Chinese Academy of Medical Sciences and Peking Union Medical College, Beijing 100021, China; [5]Department of Anesthesiology, National Cancer Center/National Clinical Research Center for Cancer/Cancer Hospital, Chinese Academy of Medical Sciences and Peking Union Medical College, Beijing 100021, China

Received February 6, 2020; Accepted June 27, 2020; Epub August 1, 2020; Published August 15, 2020

Abstract: The expression of RNA-binding proteins (RBPs) is dysregulated in colorectal cancer (CRC) and in other types of cancer. Among the RBPs, the insulin-like growth factor-2 messenger RNA binding protein (IGF2BP1-3) family is involved in the development of the colon and the progression of CRC. However, the regulation of mRNA fate by IGF2BP3 in CRC remains less well understood. Here, we show that IGF2BP3 interacts with ELAVL1 to coregulate a cohort of genes involved in the cell cycle and cell proliferation. Mechanistically, recognition of these mRNAs by the IGF2BP3/ELAVL1 complex leads to prolonged half-lives of the mRNA molecules and increased expression of the target genes, thereby driving CRC cell proliferation. Interestingly, knockdown of either IGF2BP3 or ELAVL1 impairs the IGF2BP3/ELAVL1 complex-enhanced mRNA stability, suggesting a functional interdependency between IGF2BP3 and ELAVL1 in CRC. Our findings reveal the molecular mechanism by which IGF2BP3 regulates mRNA stability and identify the cooperativity of the IGF2BP3/ELAVL1 complex as a novel therapeutic target in CRC.

Keywords: Colorectal cancer, RBP, IGF2BP3, ELAVL1, mRNA stability

Introduction

Colorectal cancer (CRC) is one of most deadly types of cancer in the digestive tract, and it was estimated that more than 1.8 million new CRC cases and 881,000 CRC-related deaths occurred in 2018 [1]. Globally, CRC remains the third most commonly diagnosed cancer and accounts for 10% of cancer-related deaths [2]. Most CRC cases arise sporadically and are often diagnosed at advanced stages [3]. After curative treatment, CRC patients often develop recurrent disease, which is highly correlated with the unfavorable prognosis of CRC [4].

The development of CRC is well-understood and characterized by distinct genetic and epigenetic events [5]. Traditional adenoma-carcinoma carcinogenesis is first initiated by an APC mutation followed by activation of RAS or functional loss of TP53, which are further accompanied by the accumulation of different molecular alterations [2, 5-7]. Importantly, emerging evidence has shown that RNA-binding proteins (RBPs) play critical roles in colorectal cancer progression [8]. RBPs bind target RNAs to form ribonucleoprotein (RNP) complexes in both context-dependent and context-independent manners, and these RNP complexes regulate the

fate and functions of RNAs, including RNA biogenesis, stability, transport and cellular localization [9, 10].

Multiple RBPs have been implicated in the modulation of gene expression at the posttranscriptional level in CRC [11, 12]. The insulin-like growth factor-2 messenger RNA binding protein (IGF2BP) family comprises three RNA-binding proteins (IGF2BP1-3), all of which are highly expressed during both colon development and CRC progression [12, 13]. The IGF2BPs exhibit distinct RNA-recognition properties, and numerous oncogenic transcripts have been identified as functional targets of IGF2BP1/2 in CRC [12]. However, it remains largely unknown how IGF2BP3 functions in binding and regulating its target transcripts in CRC progression.

In this study, we first determined the oncogenic roles of IGF2BP3 in CRC *in vitro* and *in vivo*. Through an approach of coimmunoprecipitation (Co-IP) combined with LC-MS/MS, we showed that IGF2BP3 physically interacted with the well-defined RNA-binding protein ELAVL1. We further predicted that 3070 target transcripts were directly coregulated by these two RBPs, indicating their collaborative roles in mRNA recognition. Interestingly, loss of either ELAVL1 or IGF2BP3 impaired the IGF2BP3/ELAVL1 complex-mediated target mRNA stability. Taken together, our findings reveal the molecular mechanism by which IGF2BP3 regulates target mRNA transcripts, which could be considered a therapeutic target in CRC treatment.

Material and methods

Cell culture and transfection

The human CRC cell lines SW480, HCT116, and DLD1 were purchased from the American Type Culture Collection (ATCC) (Manassas, VA) and maintained in RPMI 1640 supplemented with 10% fetal bovine serum (FBS) (Gibco). Transient transfection of siRNA was performed with the Lipofectamine™ RNAi MAX Transfection Reagent (Invitrogen #13778150) following the standard protocol. The siRNAs used in this study were purchased from RiboBio (stB00047-45, MAP2K1; stB0008179, TPR).

RIP-qPCR assay

The RIP assay was performed using the EZ-Magna RIP Kit (Millipore #17-701). Briefly, 1× 10^7 IGF2BP3-overexpressing SW480 cells and control cells were collected. The cell pellets were resuspended in the RIP Lysis Buffer supplemented with the Protease Inhibitor Cocktail and RNase Inhibitor and incubated on ice for 5 min. The magnetic beads were washed with the RIP Wash Buffer, and then, 5 μg of RIPAb+ IGF2BP3-RIP Validated Antibody (Sigma-Aldrich #03-198) or ELAVL1 (Abcam #ab136542) antibody was added to each tube. The magnetic beads and antibodies were incubated with rotation for 30 min at room temperature. Then, the RIP lysates were added to the antibody-coated magnetic beads and incubated in tubes with rotation for 3 h to overnight at 4°C. The beads were collected and washed six times. The immunoprecipitated RNA was eluted with a proteinase K buffer, extracted with a phenol:chloroform:isoamyl alcohol l (125:24:1, pH 4.3) buffer and analyzed with quantitative RT-qPCR.

RNA extraction and quantitative RT-qPCR

Total RNA extraction was performed with the TRIzol reagent (Invitrogen #15596018) as previously described [14]. Briefly, the total RNA samples were reverse transcribed with the PrimeScript™ RT reagent Kit (Takara #RR0-37A), and RT-qPCR was performed using TB Green® Premix Ex Taq™ II (Takara #RR820A) according to the manufacturer's instructions. Each experiment was repeated independently at least three times. The primers used are listed in the Table S1.

Measurement of RNA stability

CRC cells were seeded in 6-well plates to obtain 50% confluence after 24 h. The cells were treated with 5 μg/ml actinomycin D (ApexBio #A4448) and were collected at the indicated time points. The total RNA was extracted by TRIzol reagent and analyzed by RT-qPCR. The turnover rates and half-lives of the mRNAs were estimated according to previous studies [15, 16].

Plasmid construction and lentivirus packaging

The *IGF2BP3* cDNA clone was constructed and subcloned into the pLVX-puro lenti-vector. The ELAVL1 (EX-Q0365-Lv101), MAP2K1 (EX-A0826-Lv101) and TPR (EX-Z8318-Lv101) cDNA clones were purchased from GeneCopoeia. The shRNA oligos targeting *IGF2BP3* or *ELAVL1* and a nontargeting oligo control were engineered

into the pSIH-puro lenti-vector. For pLVX-puro lentivirus production, the packaging plasmids delta 8.9 and pLP2 were used. For pSIH-puro lentivirus production, the packaging plasmids vSVG, pLP1 and pLP2 were used. The packaging plasmids and the indicated lentiviral vectors were cotransfected into HEK293T cells. After transfection for 48 h, the supernatants containing lentivirus particles were collected and stored in aliquots at -80°C. For lentivirus infection, CRC cells were first treated with polybrene (5 μg/ml) (Santa Cruz #Sc-134220) and then infected with the indicated lentivirus. Stable cell populations were established by selecting with puromycin (1 μg/ml) (Gibco #A11138-03) or neomycin (400 μg/ml) (Gibco #10131027) for 2 weeks.

Western blotting assays

Western blotting was performed as previously described [14]. Briefly, the cells were collected and lysed in lysis buffer (1% NP-40, 0.1% sodium dodecyl sulfate, 50 mM Tris-HCl pH 7.4, 150 mM NaCl, 0.5% sodium deoxycholate, 1 mM EDTA, and 1× Proteinase Inhibitor Cocktail) for 30 min on ice. Equal amounts of proteins were loaded and resolved by 10% SDS-PAGE gels and transferred onto PVDF membranes. The membranes were blocked with 5% BSA solution and then incubated with specific antibodies at 4°C overnight. Following incubation with secondary antibodies, the immunoblots were detected using Western Lightning Plus ECL (PerkinElmer #203-17071). The antibodies used for western blotting were as follows: anti-IGF2BP3 (Proteintech #14642-1-AP), anti-TPR (Abcam #ab170940), and anti-MAP2K1 (Abcam #ab32576), anti-ELAVL1 (Abcam #ab136542).

Cell proliferation assays

Cell proliferation was quantified by CCK-8 assays. CRC cells were seeded into 96-well plates (2×10^4 cells/ml; 100 μl/well). The Cell Proliferation Reagent CCK-8 (Dojindo Molecular Technologies #CK04) was used to measure cell proliferation. After 2 h of incubation, the absorbance was measured at 450 nm using a microplate reader.

Colony formation assays

HCT116/DLD1 cells (2×10^3) or SW480 cells (1×10^4) with indicated treatment were seeded in 6-well plates. After 5-7 days, the cells were fixed with methanol followed by crystal violet staining. The colonies were counted in three random fields under a microscope. All the experiments were performed at least three times in triplicate.

Immunoprecipitation and mass spectrometry

For immunoprecipitation, 900 μg of protein was incubated with specific antibodies (2-3 μg) overnight at 4°C with rotation. Then, 30 μL anti-FLAG M2 affinity gel (Sigma) was added, and the incubation was continued for an additional 2 h. The beads were then washed 5 times using Buffer CF 0.15 (1 M HEPES, pH 7.9, glycerol, 5 M NaCl, 2 M $MgCl_2$, 0.5 M EDTA, 10% NP 40, 1 M DTT, and 250 mM PMSF). The precipitated proteins were eluted from the beads by resuspending the beads in 2× SDS-PAGE loading buffer and boiling for 10 min. The eluted proteins were then analyzed by western blotting. For mass spectrometry, the proteins harvested from the immunoprecipitation were separated with 10% SDS-PAGE gels followed by silver staining according to the manufacturer's protocol (Beyotime #P0017S). The desired bands were excised and subjected to LC-MS/MS sequencing and analysis. The result of mass spectrometry is listed in the Table S2.

Mouse xenograft studies

Six-week-old male BALB/c nude mice were purchased from Vital River (Beijing, China). Stable IGF2BP3-deficient HCT116 and DLD1 cells (1×10^6) were subcutaneously injected into the BALB/c nude mice. The tumor volumes were measured every four days, and the tumor masses were harvested and weighed 2-3 weeks after the initial cell implantation. All the procedures and experimental protocols were approved by the Institutional Animal Care and Use Committee of the Chinese Academy of Medical Sciences Cancer Hospital.

Immunohistochemistry analysis

Human CRC tissue microarrays were purchased from Servicebio Company (G6037-3). This study was approved by the ethical committee of the hospital, and informed consent was obtained from each enrolled patient. The tissue microarrays were stained with the anti-IGF2BP3 antibody (Proteintech #14642-1-AP) following the IHC procedure that was previously described [17]. The images were captured by

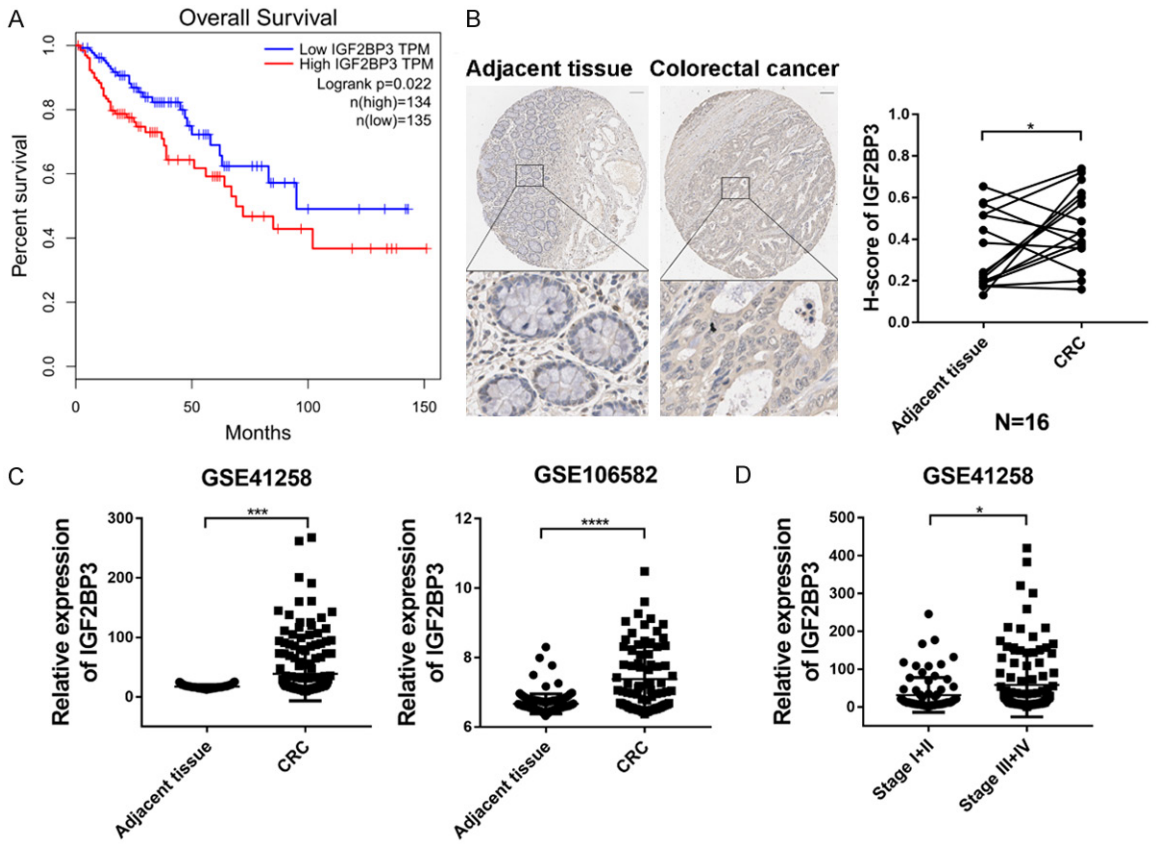

Figure 1. Analysis of clinical significance of IGF2BP3 in CRC. (A) Kaplan-Meier analysis of CRC patient survival with the GEPIA database [18] in strata defined according to high or low expression of IGF2BP3. (B) Representative images of IHC staining for IGF2BP3 in colorectal normal tissues and colorectal cancer tissues. Scale bar, 100 μm (left panel). The IHC score of IGF2BP3 was markedly higher in the CRC tissues than in the adjacent normal tissues (N=16) (right panel). (C) The mRNA level of *IGF2BP3* was analyzed in two independent CRC patient cohorts, GSE41258 (left panel) and GSE106582 (right panel), showing that the *IGF2BP3* mRNA levels were increased in the CRC tissues compared to the paired adjacent tissues. (D) The mRNA level of *IGF2BP3* was analyzed in CRC patients (GSE41258) with higher or lower stage. **P<0.05*, ****P<0.001*, *****P<0.0001.*

an Aperio ScanScope (Leica, Nussloch, Germany).

Statistical analysis

Data analysis was conducted using GraphPad Prism (Version 6). The data was reported as the mean ± S.D. Statistical significance was calculated using two-sided Student's t-tests or Wilcoxon matched-pairs signed rank test. ANOVA or the Friedman test was used for statistical analysis in multiple experimental groups. A *P*-value <0.05 was considered statistically significant.

Results

IGF2BP3 is overexpressed in CRC

To investigate the roles of IGF2BP3 in CRC, we first examined the expression of IGF2BP3 and its correlation with the clinical outcomes of colorectal cancer patients. In a cohort of 269 CRC patients from TCGA database [18], we found that high expression of IGF2BP3 was associated with worse overall survival of CRC patients (**Figure 1A**). Next, we measured the expression of IGF2BP3 in 16 paired patient samples of CRC tissue and adjacent normal tissue with immunohistochemistry (IHC). Consistent with previous findings that the expression of IGF2BP3 was significantly increased in CRC [19, 20], higher expression of IGF2BP3 was observed in the cytoplasm and membrane of CRC cells. The H-scores of IGF2BP3 were markedly increased in the CRC tissues compared to the paired normal tissues (N=16) (**Figure 1B**). These findings were further validated in the two cohorts of CRC patients from the GEO databases (**Figure 1C**). Importantly, the IGF2BP3 levels significantly increased with CRC progression from early to late stages (**Figure 1D**). Taken together, these data sug-

gest that IGF2BP3 expression is aberrantly increased in CRC tissues and strongly correlated with CRC malignancy.

IGF2BP3 promotes CRC cell proliferation in vitro and in vivo

To further delineate the functional roles of IGF2BP3 in CRC, we first analyzed the expression of IGF2BP3 in CRC cells. As shown in Figure S1A, the mRNA expression of IGF2BP3 was much higher in the four CRC cell lines than in the normal colon FHC cell line, which was supportive of the oncogenic role of IGF2BP3 in the CRC cell model. We further analyzed the protein level of the four CRC cell lines (Figure S1B) and found that the HCT116 and DLD1 cells harbored relatively high expression of IGF2BP3 compared to the SW480 and HT29 cells. To investigate the functions of IGF2BP3 in CRC, we first infected SW480 cells with lentivirus encoding IGF2BP3 and then examined the cell viability of both the IGF2BP3-overexpressing cells and control cells. We found that the ectopic overexpression of IGF2BP3 dramatically promoted the proliferation and survival of the SW480 cells (**Figures 2A-C**, S1C). We also generated stable IGF2BP3-deficient HCT116 and DLD1 cell lines with lentivirus carrying shRNA targeting IGF2BP3 (shIGF2BP3 #1-#4) or non-targeting shCtrl as a control (Figure S1D-G). Consistently, stable knockdown of IGF2BP3 significantly suppressed the proliferation and survival of both cell lines (**Figure 2D-G**). To further demonstrate the growth-promoting effect of IGF2BP3 *in vivo*, we subcutaneously injected the stable IGF2BP3-deficient HCT116 and DLD1 cells and control cells into BALB/c nude mice. Compared to the control cells, knockdown of IGF2BP3 in both cell lines significantly inhibited the tumor growth and decreased the tumor weights (**Figure 2H-K**). Together, these results clearly reveal that IGF2BP3 drives CRC cell proliferation *in vitro* and outgrowth *in vivo*.

IGF2BP3 physically interacts with the RNA binding protein ELAVL1 to recognize common mRNA transcripts in CRC

Given that RNA binding proteins are able to interact with multiple protein partners to regulate downstream targets [21-23], we proposed that IGF2BP3 recognized and regulated mRNA transcripts through potential collaborative interactions with other proteins. To validate this hypothesis, we first employed affinity purification and mass spectrometry to determine the IGF2BP3 interactome *in vivo*. In detail, FLAG-tagged IGF2BP3 (FLAG-IGF2BP3) was stably expressed in SW480 cells (Figure S2A). Whole-cell extracts were then collected and subjected to affinity purification using an anti-FLAG affinity gel. The purified protein complex was analyzed by western blotting followed by silver staining (**Figures 3A**, S2A). Through mass spectrometric analysis, we identified 449 IGF2BP3-interacting proteins in total, 436 of which were IGF2BP3-specific protein targets (Figure S2B). GO analysis of the IGF2BP3-specific binding targets further indicated that most of them were implicated in multiple activities related to RNA regulation (Figure S2C, S2D). Accordingly, IGF2BP3 was copurified with the well-defined RNA-binding protein ELAVL1 (**Figure 3A**), and this interaction was confirmed by coimmunoprecipitation (Co-IP) in FLAG-IGF2BP3-expressing SW480 cells (**Figure 3B**). Reciprocally, IP with an antibody against ELAVL1 followed by western blotting analysis also showed that IGF2BP3 was efficiently coimmunoprecipitated by ELAVL1 in HCT116 cells (**Figure 3C**).

To identify the mRNA transcripts that are coregulated by these two RBPs, we then searched the online RBP database, which provided both IGF2BP3 and ELAVL1 CLIP-seq data [24]. Surprisingly, we found that 3070 mRNA transcripts were coregulated by IGF2BP3 and ELAVL1 (**Figure 3D**), which implied that IGF2BP3 may cooperate with ELAVL1 to modulate the functions of these mRNAs. GO analysis revealed that these common mRNA targets were involved in the cell cycle transition and cell proliferation (Figure S2E). Next, we performed an RIP assay in IGF2BP3-overexpressing SW480 cells to validate the binding of IGF2BP3 to four randomly selected mRNA transcripts (*KRAS, MAP2K1, TPR,* and *CCNH*). As expected, in IGF2BP3-overexpressing SW480 cells, we observed increased IGF2BP3 bindings to these mRNA transcripts (**Figure 3E**). Finally, we proposed that IGF2BP3 interacting with ELAVL1 recognized and bound to these mRNAs. Based on the RIP assay, we observed increased enrichment of ELAVL1 on these mRNA transcripts, implying collaborative roles of these two RBPs in binding to target mRNAs (**Figure 3F**). Taken together, these findings reveal that

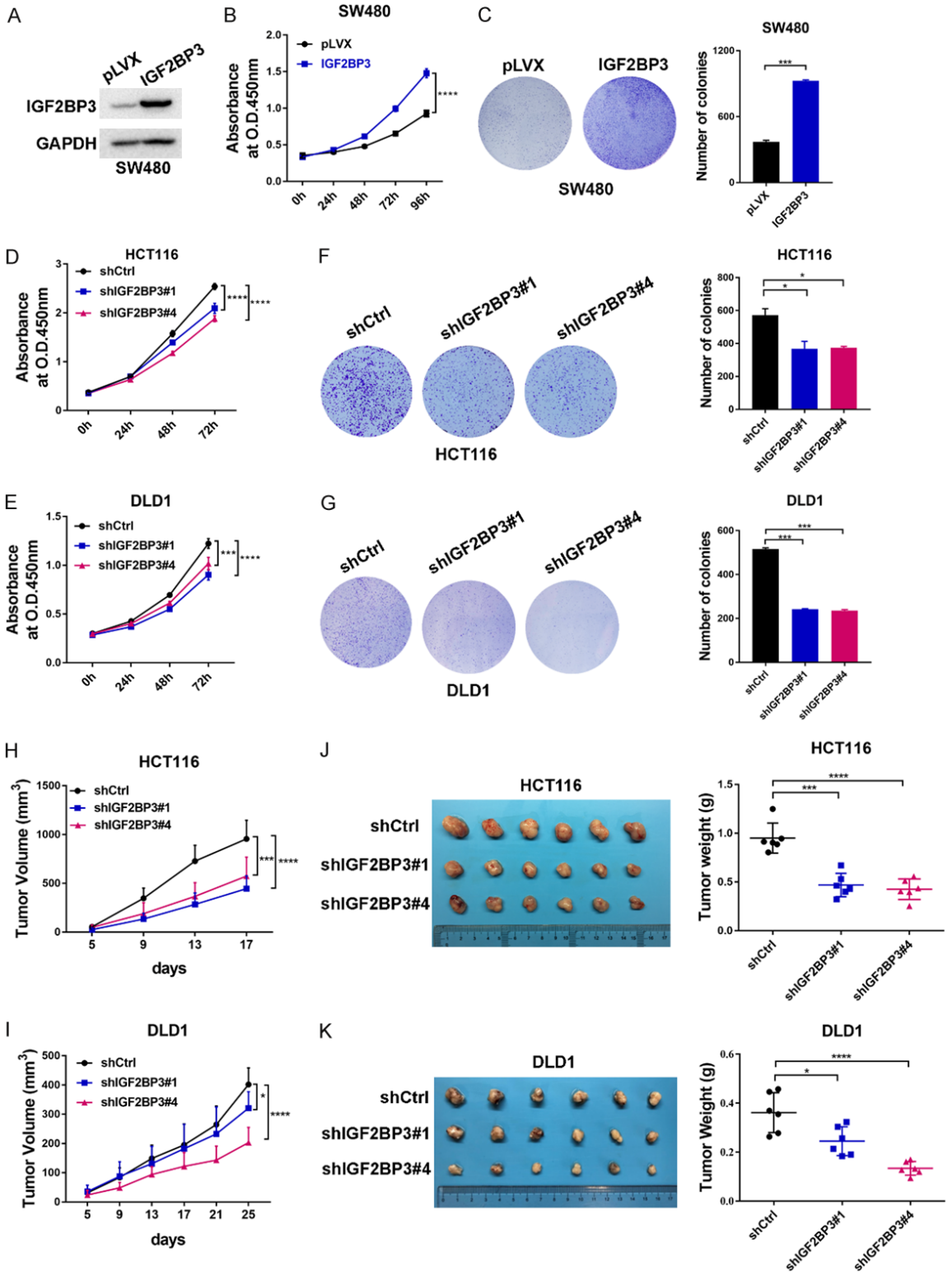

Figure 2. Oncogenic roles of IGF2BP3 in CRC. (A) Establishment of IGF2BP3-overexpressing SW480 cells. The expression of IGF2BP3 was analyzed with western blotting analysis. (B) Cell proliferation assays were performed in the IGF2BP3-overexpressing SW480 cells and control cells. (C) A total of 10,000 IGF2BP3-overexpressing SW480 cells and control cells were seeded into 6-well plates, and the colony formation ability of each group was assessed. Representative images are shown in (C) (left panel). The results were quantitatively analyzed (right panel). (D, E) Cell proliferation assays were performed in the stable IGF2BP3-deficient HCT116 (D) and DLD1 (E) cells and control

cells. (F, G) A total of 2,000 stable IGF2BP3- deficient HCT116 (F) and DLD1 (G) cells and control cells were seeded into 6-well plates, and the colony formation ability of each group was assessed. Representative images are shown in (F and G) (left panel). The results were quantitatively analyzed (right panel). (H-K) Stable IGF2BP3-depleted HCT116 (H) or DLD1 (I) cells and control cells were subcutaneously injected into male BALB/c nude mice. The tumor growth was measured (H, I). Representative images are shown (J, K left panel), and the tumor weights from each group were statistically analyzed (J, K right panel). **P<0.05, ***P<0.001, ****P<0.0001.*

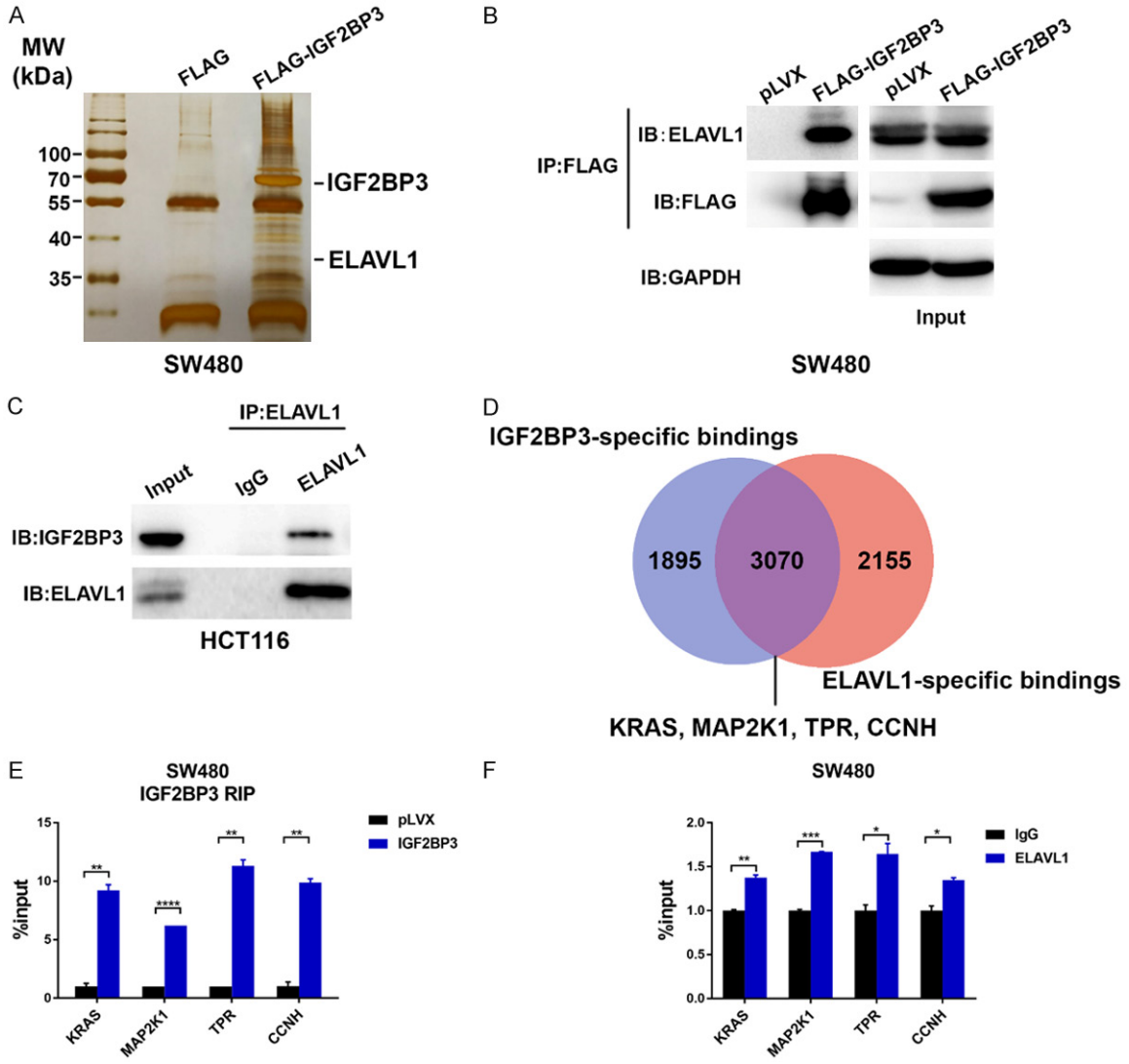

Figure 3. Identification of IGF2BP3-interacted proteins and target mRNAs. (A) Cellular extracts from the SW480 cells stably expressing FLAG (control) or FLAG-IGF2BP3 were immunoprecipitated with an anti-FLAG M2 affinity gel and eluted with 2x loading buffer. The protein eluates were resolved by 10% SDS-PAGE gel electrophoresis and silver-stained. The indicated protein bands were retrieved for mass spectrometry analysis. (B) Whole-cell lysates from the FLAG-IGF2BP3-overexpressing SW480 cells and control cells were prepared, and co-IP was performed with an anti-FLAG M2 affinity gel. The immunoprecipitates were then blotted using antibodies against the indicated proteins. (C) Whole-cell lysates from HCT116 cells were prepared, and co-IP was performed with an antibody against ELAVL1. The immunoprecipitates were then analyzed by using antibodies against the indicated proteins. (D) Analysis of the potential overlapping mRNA targets of IGF2BP3 and ELAVL1 according to the Starbase database (http://starbase.sysu.edu.cn). (E) RIP analysis was performed to validate the binding of IGF2BP3 to the regulatory regions of the *KRAS, MAP2K1, TPR,* and *CCNH* mRNA transcripts in the IGF2BP3-overexpressing SW480 cells and control cells. (F) RIP analysis was performed to validate the binding of ELAVL1 to the regulatory regions of the *KRAS, MAP2K1, TPR, and CCNH* mRNA transcripts in SW480 cells. ***P<0.01, ****P<0.0001.*

IGF2BP3 physically interacts with ELAVL1 to recognize mRNA transcripts in CRC cells.

IGF2BP3 synergizes with ELAVL1 to regulate mRNA stabilization in CRC

Previous studies showed that RBPs bind to target mRNA transcripts to regulate mRNA stability [10]. We next tested the stability of mRNAs bound by both IGF2BP3 and ELAVL1 by calculating the half-lives of these mRNAs. Both IGF2BP3-overexpressing SW480 cells and control cells were treated with actinomycin D for 60 min and 80 min respectively followed by the quantification of the relative mRNA levels. We found that overexpression of IGF2BP3 significantly increased the half-lives of these four selected mRNA transcripts (*KRAS, MAP2K1, TPR* and *CCNH*) (**Figure 4A**), indicating that IGF2BP3 plays critical roles in regulating mRNA stability in CRC cells. Among these transcripts, the half-lives of MAP2K1 and TPR mRNA almost doubled in the IGF2BP3-expressing SW480 cells (**Figures 4B**, **4C**, S3A, S3B). RT-qPCR analysis further revealed that the mRNA levels of these genes were significantly increased in the IGF2BP3-overexpressing SW480 cells compared to the control cells (**Figures 4D**, S3C). Conversely, knockdown of IGF2BP3 in HCT116 cells significantly decreased the mRNA levels of these genes (**Figures 4E**, S3D). IGF2BP3 contains two RRMs and four KH domains, The C-terminal KH domains (KH) of the IGF2BP3 are indispensable for target RNA-binding, whereas the RRM domains mediate protein-RNA complexes stabilization as well as association with other RBPs [25]. We next constructed different IGF2BP3 truncated mutants to examine which domains were essential for target mRNA stability (**Figure 4F**, **4G**). We found that deletion of KH domains (KH1-4), but not the RRM domains, significantly decreased the mRNAs stability of four indicated genes compared to IGF2BP3 wide-type control. Interestingly, deletion of either KH1-2 or KH3-4 domain of IGF2BP3 retained the abilities to stabilize target mRNAs. These data suggested that the KH domains are required for IGF2BP3-mediated mRNA stabilization (**Figures 4H**, **4I**, S3E, S3F). Consistently, overexpression of IGF2BP3 with KH domains deletion (KH1-4) exhibited no effect on SW480 cell proliferation, whereas other deletion mutants remained the growth-promoting effects (**Figure 4J**). In summary, KH domains of IGF2BP3 are indispensable for target mRNA stability and cell proliferation in CRC.

Given that ELAVL1 was colocalized with IGF2BP3 and bound to the same set of mRNA targets (**Figure 3**), we next investigated if ELAVL1 was able to affect the stability of these mRNAs. We stably knocked down the expression of ELAVL1 in the IGF2BP3-overexpressing SW480 cells (**Figures 5A**, S4A). Interestingly, in the IGF2BP3-overexpressing SW480 cells, knockdown of ELAVL1 significantly decreased the enhanced bindings of IGF2BP3 to mRNAs, leading to attenuated mRNA stability and decreased mRNA expression (**Figures 5B-F**, S4B-F). These data suggested that ELAVL1 is indispensable for the regulation of mRNA stability by IGF2BP3. Similarly, when IGF2BP3 was depleted in ELAVL1-overexpressing HCT116 cells (Figure S4G, S4H), ELAVL1-regulated mRNA stability was also significantly reduced (Figure S4I-L). Moreover, the expression of IGF2BP3 was positively correlated with ELAVL1 in CRC patient tissues (Figure S4M). Taken together, these data suggest IGF2BP3 synergizes with ELAVL1 to regulate downstream mRNAs.

Finally, we sought to determine the clinical correlations between IGF2BP3/ELAVL1 and their regulated targets in CRC. We found that the expression of both MAP2K1 and TPR was positively correlated with IGF2BP3 or ELAVL1 in CRC patient tissues (**Figure 5G-J**), demonstrating functional dependency and clinical significance between IGF2BP3/ELAVL1 and MAP2K1/TPR in CRC. Taken together, our findings suggest that IGF2BP3 increases mRNA stability through collaborative interaction with ELAVL1 in CRC.

Loss of MAP2K1 or TPR impairs IGF2BP3-driven cell proliferation in CRC

Given that the expression of MAP2K1 and TPR was strongly correlated with IGF2BP3 or ELAVL1 in the CRC specimens, we next examined the functions of these two genes in CRC. By analyzing two CRC patient cohorts from the GEO datasets, we found that the mRNA expression of these two genes was markedly upregulated in CRC patient tissues compared to adjacent tissues (**Figure 6A**, **6B**). Additionally, transient silencing of these two genes in HCT116 and DLD1 cells with small interfering RNA

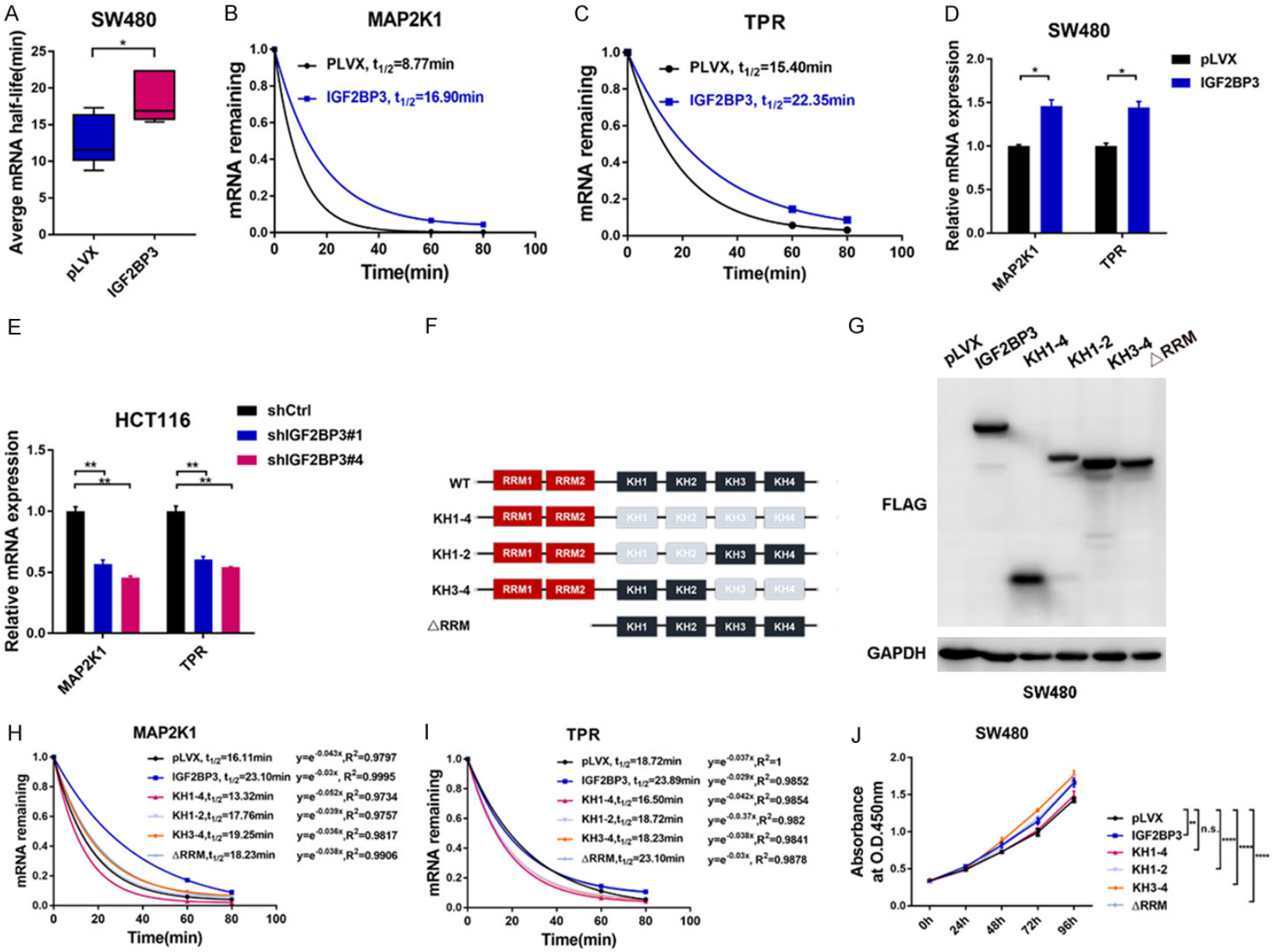
A
SW480
Averge mRNA half-life(min)
pLVX
IGF2BP3
B
MAP2K1
mRNA remaining
PLVX, t1/2=8.77min
IGF2BP3, t1/2=16.90min
Time(min)
C
TPR
mRNA remaining
PLVX, t1/2=15.40min
IGF2BP3, t1/2=22.35min
Time(min)
D
SW480
Relative mRNA expression
pLVX
IGF2BP3
MAP2K1
TPR
E
HCT116
Relative mRNA expression
shCtrl
shIGF2BP3#1
shIGF2BP3#4
MAP2K1
TPR
F
WT
KH1-4
KH1-2
KH3-4
△RRM
RRM1
RRM2
KH1
KH2
KH3
KH4
G
pLVX
IGF2BP3
KH1-4
KH1-2
KH3-4
△RRM
FLAG
GAPDH
SW480
H
MAP2K1
mRNA remaining
pLVX, t1/2=16.11min y=e-0.043x,R2=0.9797
IGF2BP3, t1/2=23.10min y=e-0.03x, R2=0.9995
KH1-4,t1/2=13.32min y=e-0.052x,R2=0.9734
KH1-2,t1/2=17.76min y=e-0.039x,R2=0.9757
KH3-4,t1/2=19.25min y=e-0.036x,R2=0.9817
△RRM,t1/2=18.23min y=e-0.038x,R2=0.9906
Time(min)
I
TPR
mRNA remaining
pLVX, t1/2=18.72min y=e-0.037x,R2=1
IGF2BP3, t1/2=23.89min y=e-0.029x,R2=0.9852
KH1-4,t1/2=16.50min y=e-0.042x,R2=0.9854
KH1-2,t1/2=18.72min y=e-0.037x,R2=0.982
KH3-4,t1/2=18.23min y=e-0.038x,R2=0.9841
△RRM,t1/2=23.10min y=e-0.03x, R2=0.9878
Time(min)
J
SW480
Absorbance at O.D.450nm
0h
24h
48h
72h
96h
pLVX
IGF2BP3
KH1-4
KH1-2
KH3-4
△RRM
n.s.

Figure 4. Analysis of IGF2BP3-mediated mRNA stability. (A) Analysis of the average mRNA half-lives of *KRAS, MAP2K1, TPR and CCNH* in the SW480 cells stably overexpressing IGF2BP3 and the control cells. (B, C) Both the IGF2BP3-overexpressing SW480 cells and control cells were treated with actinomycin D for 60 and 80 min respectively. Total RNA was extracted, the relative expression of *MAP2K1* (B) and *TPR* (C) was calculated, and the mRNA half-lives of these genes were analyzed. (D) RT-qPCR analysis was performed to analyze the mRNA expression of *MAP2K1* and *TPR* in the SW480 cells stably overexpressing IGF2BP3 and the control cells. (E) RT-qPCR analysis was performed to analyze the mRNA expression of *MAP2K1* and *TPR* in the IGF2BP3-deficient HCT116 cells and control cells. (F) Schematic graph depicts the RNA-binding domains of IGF2BP3 and indicated deletions mutants constructed for the following study. (G) Western blot analysis showed the molecular weights of indicated IGF2BP3 deletion mutants. (H, I) The indicated IGF2BP3 deletion mutants and IGF2BP3 (WT) were stably overexpressed in SW480 cells. Cells were treated with actinomycin D for 60 and 80 min respectively. Total RNA was extracted, the relative expression of *MAP2K1* (H) and *TPR* (I) was calculated, and the mRNA half-lives of these genes were analyzed. (J) The indicated IGF2BP3 deletion mutants and IGF2BP3 (WT) were stably overexpressed in SW480 cells and a CCK-8 assay was performed to measure the cell proliferation in the indicated groups. **P<0.05*, ***P<0.01*, *****P<0.0001.*

(siRNA) significantly suppressed cell proliferation *in vitro*, which confirmed the oncogenic roles of these two genes (**Figures 6C**, **6D**, S5A-F). To further verify that IGF2BP3 is an upstream regulator of these two onco-transcripts, we transiently transfected siRNA targeting MAP2K1 or TPR into the IGF2BP3-overexpressing SW480 cells and examined cell proliferation in each group. As ectopic expression of IGF2BP3 in SW480 cells enhanced its binding to these two mRNAs and led to increased mRNA stability (**Figures 3E**, **4B**, **4C**), we further determined that the mRNA expression of MAP2K1 and TPR was increased in the IGF2BP3-overexpressing SW480 cells and was decreased after siRNA-mediated gene silencing (**Figure 6E**, **6F**). Consistently, the cell proliferation of the SW480 cells was dramatically increased by IGF2BP3 overexpression, and this increase was counteracted by the silencing of its downstream effector MAP2K1 or TPR (**Figure 6E**, **6F**). Reciprocally, the ectopic expression of MAP2K1 or TPR was sufficient to rescue the proliferative abilities of the IGF2BP3-depleted HCT116 or DLD1 cells (Figure S6A-H). Collectively, these data clearly demonstrate that MAP2K1 and TPR act as direct targets of IGF2BP3 to exert protumorigenic functions in CRC.

Discussion

Sequence-specific RNA-binding proteins (RBPs) recognize and interact with a large number of RNAs to form ribonucleoproteins (RNPs), thereby controlling the fate of these RNAs [9-11]. Increasing evidence shows that RBPs are dysregulated in many human cancers and play crucial roles in cancer development [8, 26]. Of note, many RBPs are implicated in the maintenance of intestinal epithelial homeostasis and the progression of colorectal cancer [12]. Among the RBPs that are critically involved in CRC development, our study focused on one of the IGF2BP family members, IGF2BP3, which has been shown to be functional in multiple cancer types [13, 25]. However, there is still limited evidence regarding its RNA binding properties. Previous findings showed that the expression of IGF2BP3 is highly correlated with unfavorable prognosis in CRC patients and that IGF2BP3 promotes CRC cells malignant progression [19, 27]. However, the mechanism by which IGF2BP3 modulates the fates of its target RNAs in CRC development remains largely unexplored.

Indeed, IGF2BP3 is overexpressed in CRC tissues compared to normal tissues (**Figure 1B**, **1C**). Functional studies also further support the tumorigenic role of IGF2BP3 in both CRC cells and xenograft models (**Figure 2**). Given that different RBPs are able to bind to the same RNA targets and exert concordant or diverse effects on the target RNAs [21-23], we next performed an IP-based LC-MS/MS assay to characterize the IGF2BP3-interacting proteins in CRC cells. Interestingly, numerous IGF2BP3-bound proteins are involved in RNA binding and processing (Figure S2B-D), suggesting that IGF2BP3 may interact with other RBPs to regulate mRNAs. This notion prompts us to discover ELAVL1, a well-characterized oncogenic RBP in multiple cancer types [11, 28]. ELAVL1 is a ubiquitously expressed member of the ELAVL protein family, which contains three RNA-binding domains to selectively bind to cis-acting AU-rich elements (AREs) and stabilize ARE-containing mRNAs to regulate target gene expression [28, 29]. Reportedly, IL-18 can induce the interaction between IGF2BP3 and ELAVL1, leading to COX-2 mRNA stabilization in acute myeloid leukemia [30]. Interestingly, all the IG-

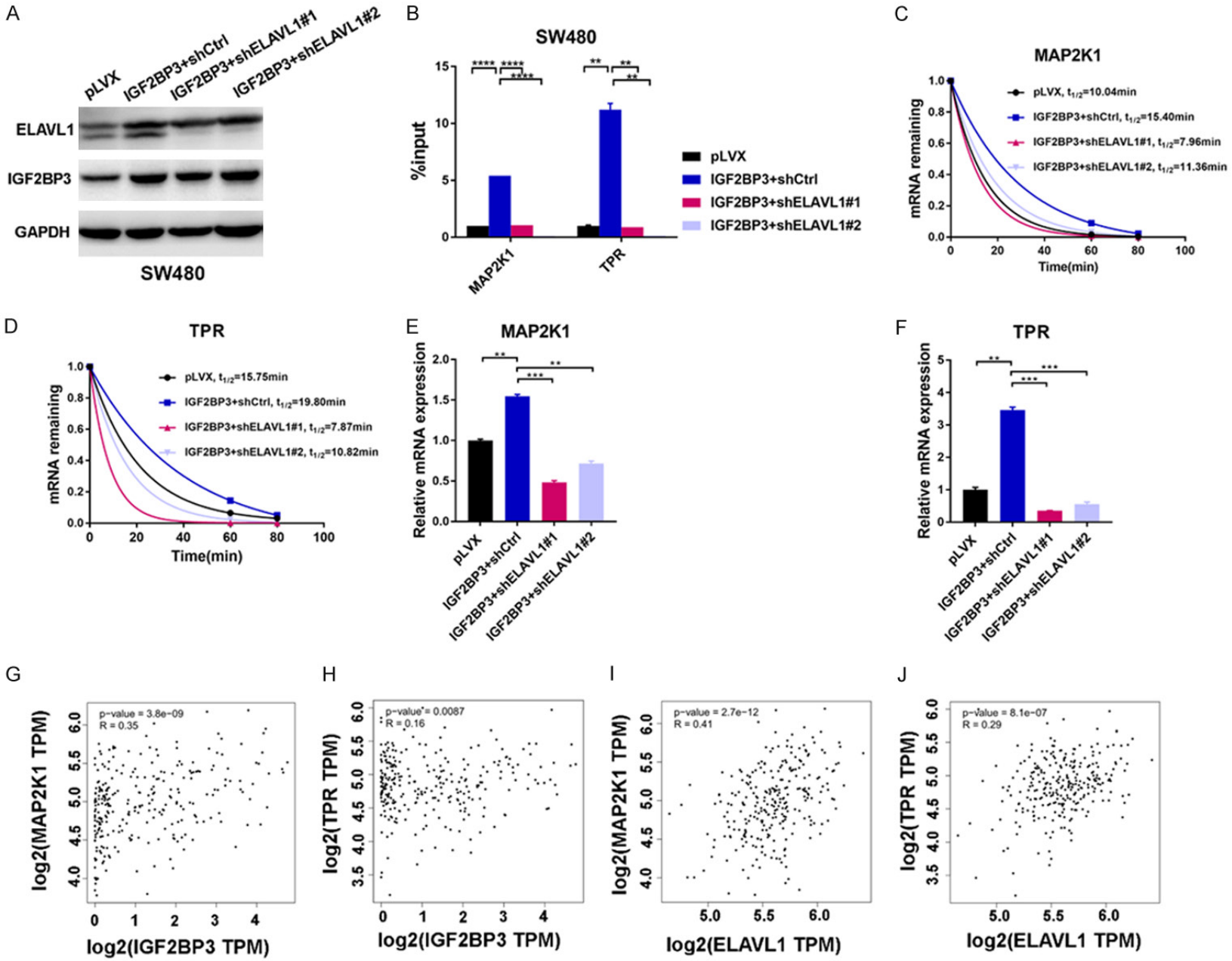
A
pLVX
IGF2BP3+shCtrl
IGF2BP3+shELAVL1#1
IGF2BP3+shELAVL1#2
ELAVL1
IGF2BP3
GAPDH
SW480
B
SW480
%input
MAP2K1
TPR
pLVX
IGF2BP3+shCtrl
IGF2BP3+shELAVL1#1
IGF2BP3+shELAVL1#2
C
MAP2K1
mRNA remaining
pLVX, t1/2=10.04min
IGF2BP3+shCtrl, t1/2=15.40min
IGF2BP3+shELAVL1#1, t1/2=7.96min
IGF2BP3+shELAVL1#2, t1/2=11.36min
Time(min)
D
TPR
mRNA remaining
pLVX, t1/2=15.75min
IGF2BP3+shCtrl, t1/2=19.80min
IGF2BP3+shELAVL1#1, t1/2=7.87min
IGF2BP3+shELAVL1#2, t1/2=10.82min
Time(min)
E
MAP2K1
Relative mRNA expression
pLVX
IGF2BP3+shCtrl
IGF2BP3+shELAVL1#1
IGF2BP3+shELAVL1#2
F
TPR
Relative mRNA expression
pLVX
IGF2BP3+shCtrl
IGF2BP3+shELAVL1#1
IGF2BP3+shELAVL1#2
G
p-value = 3.8e-09
R = 0.35
log2(MAP2K1 TPM)
log2(IGF2BP3 TPM)
H
p-value = 0.0087
R = 0.16
log2(TPR TPM)
log2(IGF2BP3 TPM)
I
p-value = 2.7e-12
R = 0.41
log2(MAP2K1 TPM)
log2(ELAVL1 TPM)
J
p-value = 8.1e-07
R = 0.29
log2(TPR TPM)
log2(ELAVL1 TPM)

Figure 5. ELAVL1 facilitates IGF2BP3-regulated mRNA stability. (A) Establishment of IGF2BP3-overexpressing SW480 cells with stable ELAVL1 depletion. The expression of ELAVL1 and IGF2BP3 was analyzed by western blotting. (B) RIP analysis was performed to analyze the binding of IGF2BP3 to the regulatory regions of the *MAP2K1* and *TPR* mRNAs in the SW480 cells overexpressing IGF2BP3 and these cells with the additional stable depletion of ELAVL1. (C, D) Analysis of the mRNA half-lives of *MAP2K1* (C) and *TPR* (D) in the SW480 cells overexpressing IGF2BP3 and these cells with the additional stable depletion of ELAVL1. (E, F) The mRNA expression of *MAP2K1* (E) and *TPR* (F) in the IGF2BP3-overexpressing SW480 cells and these cells with the additional stable depletion of ELAVL1 was analyzed with RT-qPCR assay. (G-J) Analysis of the clinical correlations between IGF2BP3/ELAVL1 and MAP2K1/TPR expression with the GEPIA database [18]. ***P<0.01*, ****P<0.001*, *****P<0.0001.*

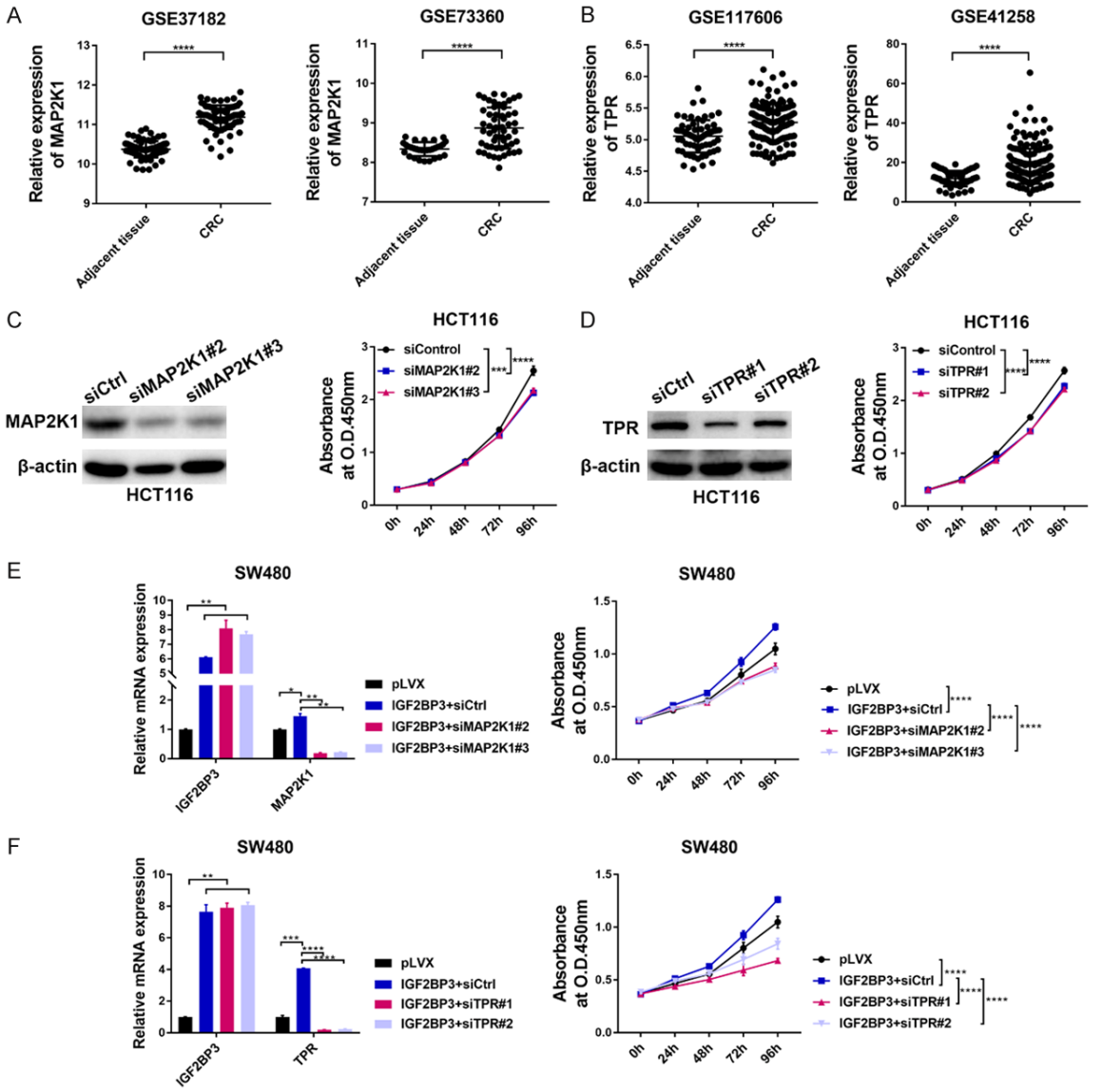

Figure 6. Functional characterizations of two IGF2BP3-regulated targets in CRC. (A, B) The mRNA levels of *MAP2K1* (A) and *TPR* (B) were analyzed in two independent CRC patient cohorts. (C) HCT116 cells were transfected with siRNA targeting *MAP2K1* and a nontargeting siRNA control, and the knockdown efficiency of MAP2K1 was confirmed by western blotting analysis (left panel). The effect of MAP2K1 silencing on the proliferation of HCT116 cells was analyzed with a CCK-8 assay (right panel). (D) HCT116 cells were transfected with siRNA targeting *TPR* and a nontargeting siRNA control, and the knockdown efficiency of TPR was confirmed by western blotting analysis (left panel). The effect of TPR silencing on the proliferation of HCT116 cells was analyzed with a CCK-8 assay (right panel). (E, F) The SW480 cells overexpressing IGF2BP3 were further transfected with siRNA targeting *MAP2K1* (E) and *TPR* (F). The expression of *IGF2BP3*, *MAP2K1* and *TPR* was analyzed with RT-qPCR analysis (E, F left panel). The proliferation of the indicated cells was examined with a CCK-8 assay (E, F right panel). **P<0.05*, ***P<0.01*, ****P<0.001*, *****P<0.0001.*

F2BP family members, IGF2BP1-3, were also confirmed to interact and colocalized with ELAVL1 in HeLa cells [16]. These findings may indicated that ELAVL1 binds to specific domains that share structural similarities among the IGF2BP family members and that might be conserved in different cell types. In our study, we predicted that 3070 mRNAs were coregulated by these two RBPs and identified two clinically relevant oncogenes (TPR and MAP2K1) in CRC (**Figure 3D-F**), suggesting a functional interplay between RBPs to cooperatively regulate the same target mRNAs.

Many cellular factors and regulatory mechanisms contribute to the stability of mRNA [31]. Generally, the mechanism of mRNA decay comprises two types: mRNA surveillance pathways that target aberrant mRNAs and mRNA half-life regulation that changes the abundance of proteins [31, 32]. ARE-mediated mRNA decay is one of the most well-defined mechanisms that governs the stability of ARE-containing mRNAs. ARE-bound ELAVL1 potentially antagonizes mRNA degradation by competing with the binding sites of the destabilizing proteins TTP, BRF1, KSRP and AUF1 [29, 32-34]. Thus, we proposed that the stability of the mRNAs that were coregulated by IGF2BP3/ELAVL1 was facilitated by ELAVL1. Consistently, loss of ELAVL1 significantly compromised the mRNA binding efficacy of IGF2BP3, leading to shortened mRNA half-lives and decreased mRNA expression levels (**Figure 5A-F**). Additionally, the mRNA fate was also regulated by posttranscriptional modifications of mRNAs. The N^6-methyladenosine (m^6A) modification has been identified as most abundant internal modification, which is enriched in 3' untranslated regions (UTRs) and close to the stop codons of target mRNA [35]. Recent study showed that IGF2BP family members functioned as m^6A readers through its KH domains (KH), which recognized and promoted mRNA stability in m^6A-dependent manner [16]. Our findings indicated the relationship between IGF2BP3 and ELAVL1 was interdependent and synergistic (**Figures 5**, S4), and the crosstalk between IGF2BP3 and ELAVL1 mediated mRNA stability remained to be further investigated.

In summary, our study reveals that the IGF2BP3/ELAVL1 complex is essential in regulating oncogenic mRNA stability in CRC. Due to the complexity of gene regulation at the posttranscriptional level, the comprehensive characterization of IGF2BP3/ELAVL1 complex-mediated mRNA stability will help provide novel molecular insights into the functions of RBPs in RNA metabolism.

Acknowledgements

This work was supported by the National Natural Science Foundation of China (No. 818-72038, 81902503).

Disclosure of conflict of interest

None.

Abbreviations

CRC, colorectal cancer; IGF2BP3, the insulin-like growth factor-2 messenger RNA binding protein; Co-IP, coimmunoprecipitation; RBPs, RNA-binding proteins; RNP, ribonucleoprotein.

Address correspondence to: Shengkai Huang, Department of Clinical Laboratory, National Cancer Center/National Clinical Research Center for Cancer/Cancer Hospital, Chinese Academy of Medical Sciences and Peking Union Medical College, Beijing 100021, China. E-mail: huang1988@cicams.ac.cn; Liang Zou, Department of Anesthesiology, National Cancer Center/National Clinical Research Center for Cancer/Cancer Hospital, Chinese Academy of Medical Sciences and Peking Union Medical College, Beijing 100021, China. E-mail: zouliang2001@163.com; Changzhi Huang, Department of Etiology and Carcinogenesis, National Cancer Center/National Clinical Research Center for Cancer/Cancer Hospital, Chinese Academy of Medical Sciences and Peking Union Medical College, Beijing 100021, China. Tel: +86-10-87788426; Fax: +86-10-87788426; E-mail: huangcz@cicams.ac.cn

References

[1] Bray F, Ferlay J, Soerjomataram I, Siegel RL, Torre LA and Jemal A. Global cancer statistics 2018: GLOBOCAN estimates of incidence and mortality worldwide for 36 cancers in 185 countries. CA Cancer J Clin 2018; 68: 394-424.

[2] Dekker E, Tanis PJ, Vleugels JLA, Kasi PM and Wallace MB. Colorectal cancer. Lancet (London, England) 2019; 394: 1467-1480.

[3] Keum N and Giovannucci E. Global burden of colorectal cancer: emerging trends, risk fac-

tors and prevention strategies. Nat Rev Gastroenterol Hepatol 2019; 16: 713-732.
[4] van der Stok EP, Spaander MCW, Grünhagen DJ, Verhoef C and Kuipers EJ. Surveillance after curative treatment for colorectal cancer. Nat Rev Clin Oncol 2017; 14: 297-315.
[5] Grazioso TP, Brandt M and Djouder N. Diet, microbiota, and colorectal cancer. iScience 2019; 21: 168-187.
[6] Fearon ER and Vogelstein B. A genetic model for colorectal tumorigenesis. Cell 1990; 61: 759-767.
[7] Lao VV and Grady WM. Epigenetics and colorectal cancer. Nat Rev Gastroenterol Hepatol 2011; 8: 686-700.
[8] Pereira B, Billaud M and Almeida R. RNA-binding proteins in cancer: old players and new actors. Trends Cancer 2017; 3: 506-528.
[9] Hentze MW, Castello A, Schwarzl T and Preiss T. A brave new world of RNA-binding proteins. Nature reviews. Mol Cell Biol 2018; 19: 327-341.
[10] Glisovic T, Bachorik JL, Yong J and Dreyfuss G. RNA-binding proteins and post-transcriptional gene regulation. FEBS Lett 2008; 582: 1977-1986.
[11] García-Cárdenas JM, Guerrero S, López-Cortés A, Armendáriz-Castillo I, Guevara-Ramírez P, Pérez-Villa A, Yumiceba V, Zambrano AK, Leone PE and Paz-Y-Miño C. Post-transcriptional regulation of colorectal cancer: a focus on RNA-binding proteins. Front Mol Biosci 2019; 6: 65.
[12] Chatterji P and Rustgi AK. RNA binding proteins in intestinal epithelial biology and colorectal cancer. Trends Mol Med 2018; 24: 490-506.
[13] Bell JL, Wächter K, Mühleck B, Pazaitis N, Köhn M, Lederer M and Hüttelmaier S. Insulin-like growth factor 2 mRNA-binding proteins (IGF2BPs): post-transcriptional drivers of cancer progression? Cell Mol Life Sci 2013; 70: 2657-2675.
[14] Zhang Q, Li Y, Zhao M, Lin H, Wang W, Li D, Cui W, Zhou C, Zhong J and Huang C. MiR-494 acts as a tumor promoter by targeting CASP2 in non-small cell lung cancer. Sci Rep 2019; 9: 3008.
[15] Chen CY, Ezzeddine N and Shyu AB. Messenger RNA half-life measurements in mammalian cells. Methods Enzymol 2008; 448: 335-357.
[16] Huang H, Weng H, Sun W, Qin X, Shi H, Wu H, Zhao BS, Mesquita A, Liu C, Yuan CL, Hu YC, Hüttelmaier S, Skibbe JR, Su R, Deng X, Dong L, Sun M, Li C, Nachtergaele S, Wang Y, Hu C, Ferchen K, Greis KD, Jiang X, Wei M, Qu L, Guan JL, He C, Yang J and Chen J. Recognition of RNA N(6)-methyladenosine by IGF2BP proteins enhances mRNA stability and translation. Nat Cell Biol 2018; 20: 285-295.
[17] Huang S, Li Y, Yuan X, Zhao M, Wang J, Li Y, Li Y, Lin H, Zhang Q, Wang W, Li D, Dong X, Li L, Liu M, Huang W and Huang C. The UbL-UBA Ubiquilin4 protein functions as a tumor suppressor in gastric cancer by p53-dependent and p53-independent regulation of p21. Cell Death Differ 2019; 26: 516-530.
[18] Tang Z, Li C, Kang B, Gao G, Li C and Zhang Z. GEPIA: a web server for cancer and normal gene expression profiling and interactive analyses. Nucleic Acids Res 2017; 45: W98-W102.
[19] Xu W, Sheng Y, Guo Y, Huang Z, Huang Y, Wen D, Liu CY, Cui L, Yang Y and Du P. Increased IGF2BP3 expression promotes the aggressive phenotypes of colorectal cancer cells in vitro and vivo. J Cell Physiol 2019; 234: 18466-18479.
[20] Lochhead P, Imamura Y, Morikawa T, Kuchiba A, Yamauchi M, Liao X, Qian ZR, Nishihara R, Wu K, Meyerhardt JA, Fuchs CS and Ogino S. Insulin-like growth factor 2 messenger RNA binding protein 3 (IGF2BP3) is a marker of unfavourable prognosis in colorectal cancer. Eur J Cancer 2012; 48: 3405-3413.
[21] Sengupta TK, Bandyopadhyay S, Fernandes DJ and Spicer EK. Identification of nucleolin as an AU-rich element binding protein involved in bcl-2 mRNA stabilization. J Biol Chem 2004; 279: 10855-10863.
[22] Ishimaru D, Ramalingam S, Sengupta TK, Bandyopadhyay S, Dellis S, Tholanikunnel BG, Fernandes DJ and Spicer EK. Regulation of Bcl-2 expression by HuR in HL60 leukemia cells and A431 carcinoma cells. Mol Cancer Res 2009; 7: 1354-1366.
[23] Sureban SM, Murmu N, Rodriguez P, May R, Maheshwari R, Dieckgraefe BK, Houchen CW and Anant S. Functional antagonism between RNA binding proteins HuR and CUGBP2 determines the fate of COX-2 mRNA translation. Gastroenterology 2007; 132: 1055-1065.
[24] Li JH, Liu S, Zhou H, Qu LH and Yang JH. starBase v2.0: decoding miRNA-ceRNA, miRNA-ncRNA and protein-RNA interaction networks from large-scale CLIP-Seq data. Nucleic Acids Res 2014; 42: D92-D97.
[25] Lederer M, Bley N, Schleifer C and Hüttelmaier S. The role of the oncofetal IGF2 mRNA-binding protein 3 (IGF2BP3) in cancer. Semin Cancer Biol 2014; 29: 3-12.
[26] Wang ZL, Li B, Luo YX, Lin Q, Liu SR, Zhang XQ, Zhou H, Yang JH and Qu LH. Comprehensive genomic characterization of RNA-binding proteins across human cancers. Cell Rep 2018; 22: 286-298.
[27] Li D, Yan D, Tang H, Zhou C, Fan J, Li S, Wang X, Xia J, Huang F, Qiu G and Peng Z. IMP3 is a novel prognostic marker that correlates with colon cancer progression and pathogenesis. Ann Surg Oncol 2009; 16: 3499-3506.

[28] García-Mauriño SM, Rivero-Rodríguez F, Velázquez-Cruz A, Hernández-Vellisca M, Díaz-Quintana A, De la Rosa MA and Díaz-Moreno I. RNA binding protein regulation and cross-talk in the control of AU-rich mRNA fate. Front Mol Biosci 2017; 4: 71.
[29] Brennan CM and Steitz JA. HuR and mRNA stability. Cell Mol Life Sci 2001; 58: 266-277.
[30] Ko CY, Wang WL, Li CF, Jeng YM, Chu YY, Wang HY, Tseng JT and Wang JM. IL-18-induced interaction between IMP3 and HuR contributes to COX-2 mRNA stabilization in acute myeloid leukemia. J Leukoc Biol 2016; 99: 131-141.
[31] Garneau NL, Wilusz J and Wilusz CJ. The highways and byways of mRNA decay. Nature reviews. Mol Cell Biol 2007; 8: 113-126.
[32] Schoenberg DR and Maquat LE. Regulation of cytoplasmic mRNA decay. Nat Rev Genet 2012; 13: 246-259.
[33] Lal A, Mazan-Mamczarz K, Kawai T, Yang X, Martindale JL and Gorospe M. Concurrent versus individual binding of HuR and AUF1 to common labile target mRNAs. EMBO J 2004; 23: 3092-3102.
[34] Linker K, Pautz A, Fechir M, Hubrich T, Greeve J and Kleinert H. Involvement of KSRP in the post-transcriptional regulation of human iNOS expression-complex interplay of KSRP with TTP and HuR. Nucleic Acids Res 2005; 33: 4813-4827.
[35] Meyer KD, Saletore Y, Zumbo P, Elemento O, Mason CE and Jaffrey SR. Comprehensive analysis of mRNA methylation reveals enrichment in 3'UTRs and near stop codons. Cell 2012; 149: 1635-1646.

Table S1. Primers of clone, shRNA, qRT-PCR, RIP-qPCR used in this study

Clone primers	Sequences
Flag-IGF2BP3-F	CGGAATTCGCCACCATGAACAAACTGTATATCGGA
Flag-IGF2BP3-R	GCTCTAGATTACTTATCGTCGTCATCCTTGTAATCCTTCCGTCTTGACTGAGG
IGF2BP3 deletion mutants primers	Sequences
KH1-4 F	CG GAATTC GCCACC ATGAACAAACTGTATATCGGA
KH1-4 R	GCTCTAGA TTA CTTATCGTCGTCATCCTTGTAATC ACATGGTTTCTGCTTGGATAC
KH1-2	#1 F: CG GAATTC GCCACC ATGAACAAACTGTATATCGGA
	R: CCTGATTTTCTTCATACATGGTTTCTGCTT
	#2 F: AAGCAGAAACCATGT ATGAAGAAAATCAGG
	R: GCTCTAGATTACTTATCGTCGTCATCCTTGTAATCCTTCCGTCTTGACTGAGG
	#3 F: CGGAATTCGCCACCATGAACAAACTGTATATCGGA
	R: GCTCTAGATTACTTATCGTCGTCATCCTTGTAATCCTTCCGTCTTGACTGAGG
KH3-4 F	CG GAATTC GCCACC ATGAACAAACTGTATATCGGA
KH3-4 R	GCTCTAGA TTA CTTATCGTCGTCATCCTTGTAATC TTCTGATTGCTCAAACTGCGG
ΔRRM F	CG GAATTC GCCACC GAAATGGCCGCCCAGCAAAAC
ΔRRM R	GCTCTAGA TTA CTTATCGTCGTCATCCTTGTAATC CTTCCGTCTTGACTGAGG
shRNA primers	Sequences
IGF2BP3-shRNA1-F	GATCC CGGTGAATGAACTTCAGAATT CTTCCTGTCAGA AATTCTGAAGTTCATTCACCG TTTTTG
IGF2BP3-shRNA1-R	AATTCAAAAA CGGTGAATGAACTTCAGAATT TCTGACAGGAAG AATTCTGAAGTTCATTCACCG G
IGF2BP3-shRNA2-F	GATCC GAAACTTCAGATACGAAATAT CTTCCTGTCAGA ATATTTCGTATCTGAAGTTTC TTTTTG
IGF2BP3-shRNA2-R	AATTCAAAAA GAAACTTCAGATACGAAATAT TCTGACAGGAAG ATATTTCGTATCTGAAGTTTC G
IGF2BP3-shRNA3-F	GATCC TCTGCGGCTTGTAAGTCTATT CTTCCTGTCAGA AATAGACTTACAAGCCGCAGA TTTTTG
IGF2BP3-shRNA3-R	AATTCAAAAA TCTGCGGCTTGTAAGTCTATT TCTGACAGGAAG AATAGACTTACAAGCCGCAGA G
IGF2BP3-shRNA4-F	GATCC GCAGGAATTGACGCTGTATAA CTTCCTGTCAGA TTATACAGCGTCAATTCCTGC TTTTTG
IGF2BP3-shRNA4-R	AATTCAAAAA GCAGGAATTGACGCTGTATAA TCTGACAGGAAG TTATACAGCGTCAATTCCTGC G
ELAVL1-shRNA-1-F	GATCC TTGTTAGTGTACAACTCATTT CTTCCTGTCAGA AAATGAGTTGTACACTAACAA TTTTTG
ELAVL1-shRNA-1-R	AATTCAAAAA TTGTTAGTGTACAACTCATTT TCTGACAGGAAG AAATGAGTTGTACACTAACAA G
ELAVL1-shRNA-2-F	GATCC TACCAGTTTCAATGGTCATAA CTTCCTGTCAGA TTATGACCATTGAAACTGGTA TTTTTG
ELAVL1-shRNA-2-R	AATTCAAAAA TACCAGTTTCAATGGTCATAA TCTGACAGGAAG TTATGACCATTGAAACTGGTA G
qRT-PCR primers	Sequences
ELAVL1-F	GGGTGACATCGGGAGAACG
ELAVL1-R	CTGAACAGGCTTCGTAACTCAT
CCNH-F	TGTTCGGTGTTTAAGCCAGCA
CCNH-R	TCCTGGGGTGATATTCCATTACT
TPR-F	AACGCCAGCGTGAGGAATATG
TPR-R	ATTACGTGGTTACCCCTTGCT
MAP2K1-F	CAATGGCGGTGTGGTGTTC
MAP2K1-R	GATTGCGGGTTTGATCTCCAG
KRAS-F	ACAGAGAGTGGAGGATGCTTT
KRAS-R	TTTCACACAGCCAGGAGTCTT
IGF2BP3-F	CCAAGCTAGACAAGCACTAGAC
IGF2BP3-R	GCGGCCATTTCATCAGGGA
qRT-PCR primers for RIP	Sequences
CCNH-F	GAATCACTTTGGCCATGCACT
CCNH-R	TGGTAGCATGTGTGAAAATGGC
TPR-F	GGTCTGCCCAGAACGAGTAG
TPR-R	TTTGGGCATTGTTTTCTTTTTAACT
MAP2K1-F	TCTGAGGGAGAAGCACAAGA
MAP2K1-R	CAGAGCTTGATCTCCCCACG
KRAS-F	TGGTGGTGTGCCAAGACATT
KRAS-R	ACCAGTGTTAAGAGAACTAGCCA

Table S2. IGF2BP3-specific interacted protein targets

Accession	Gene Name	Mass	Score	Matches	Sequences	emPAI	Coverage
P23396	RPS3	26842	1265	118 (74)	19 (14)	7.22	0.65
Q9Y2R9	MRPS7	28230	1100	90 (49)	17 (12)	7.35	0.61
P11940	PABPC1	70854	5989	357 (230)	37 (31)	10.04	0.57
Q92552	MRPS27	47924	958	81 (43)	23 (14)	2.54	0.57
Q9P015	MRPL15	33570	487	54 (22)	16 (11)	3.12	0.53
P63244	RACK1	35511	1181	77 (45)	16 (12)	4.45	0.51
P62701	RPS4X	29807	412	56 (22)	13 (8)	2.55	0.49
P07355	ANXA2	38808	104	27 (5)	16 (5)	0.77	0.48
Q9Y6M1	IGF2BP2	66195	9165	543 (353)	30 (28)	10.28	0.47
Q9NZI8	IGF2BP1	63783	6252	431 (253)	30 (19)	5.1	0.46
P61247	RPS3A	30154	989	78 (37)	16 (9)	4.91	0.46
Q9HCE1	MOV10	114512	988	91 (46)	39 (28)	1.6	0.46
P18124	RPL7	29264	795	73 (34)	15 (10)	4.02	0.46
P82673	MRPS35	37106	1226	67 (46)	16 (13)	5.57	0.45
P67809	YBX1	35903	623	47 (20)	10 (7)	1.89	0.45
Q13310	PABPC4	71080	3578	192 (126)	29 (24)	4.32	0.44
P51398	DAP3	45880	1739	132 (84)	20 (17)	4.69	0.44
Q15717	ELAVL1	36240	790	43 (27)	12 (10)	2.12	0.44
Q9Y676	MRPS18B	29719	729	60 (33)	11 (9)	2.97	0.44
P15880	RPS2	31590	745	61 (40)	13 (10)	2	0.43
P05388	RPLP0	34423	451	39 (18)	11 (6)	1.09	0.42
P62241	RPS8	24475	664	47 (26)	8 (5)	1.79	0.41
P62906	RPL10A	24987	414	41 (16)	11 (7)	2.98	0.41
P82933	MRPS9	46034	1314	88 (48)	16 (13)	3.91	0.4
P62424	RPL7A	30148	963	47 (27)	14 (9)	2.89	0.4
P63261	ACTG1	42108	525	57 (20)	11 (6)	0.98	0.4
P82675	MRPS5	48489	506	53 (24)	19 (8)	1.35	0.39
Q92841	DDX17	80906	499	48 (23)	25 (16)	1.21	0.39
Q9UNQ2	DIMT1	35499	97	14 (5)	10 (5)	0.87	0.39
P82650	MRPS22	41425	2693	140 (100)	16 (14)	5.82	0.38
Q92665	MRPS31	45405	1879	116 (68)	19 (12)	3.07	0.38
Q02878	RPL6	32765	321	34 (15)	12 (9)	1.89	0.38
Q9H9J2	MRPL44	37854	178	21 (5)	12 (4)	0.52	0.38
Q7L2E3	DHX30	134938	1423	111 (64)	42 (33)	1.48	0.37
Q9Y399	MRPS2	33513	603	97 (38)	15 (13)	6.26	0.37
Q96DV4	MRPL38	44968	391	44 (19)	14 (9)	1.9	0.37
Q07955	SRSF1	27842	304	24 (15)	10 (6)	0.97	0.37
Q96EY7	PTCD3	79184	1776	121 (74)	25 (19)	2.12	0.36
Q9NYK5	MRPL39	39200	323	29 (16)	12 (10)	1.87	0.36
P46777	RPL5	34569	315	34 (15)	13 (8)	2.01	0.36
P22626	HNRNPA2B1	37464	111	31 (6)	11 (5)	0.53	0.36
Q13084	MRPL28	30252	77	27 (4)	9 (2)	0.87	0.36
Q6PKG0	LARP1	123833	1183	117 (45)	32 (17)	0.92	0.35
Q9NZB2	FAM120A	123008	1036	72 (37)	32 (20)	1.03	0.35
Q1KMD3	HNRNPUL2	85622	954	72 (34)	28 (17)	1.2	0.35
P16403	HIST1H1C	21352	360	23 (14)	8 (5)	1.41	0.35
Q9BZE1	MRPL37	48600	407	37 (16)	15 (10)	1.2	0.34

P82930	MRPS34	25692	226	37 (15)	10 (7)	2.4	0.34
P49406	MRPL19	33799	140	18 (8)	11 (6)	1.12	0.34
P07910	HNRNPC	33707	602	52 (23)	12 (6)	1.55	0.33
P49411	TUFM	49852	212	27 (8)	14 (6)	0.57	0.33
O76021	RSL1D1	55167	136	26 (10)	16 (9)	0.68	0.33
Q96A35	MRPL24	25013	121	23 (7)	7 (4)	0.65	0.33
P62979	RPS27A	18296	98	12 (4)	5 (2)	0.4	0.33
Q96HS1	PGAM5	32213	86	25 (9)	10 (6)	0.8	0.33
Q9Y5M8	SRPRB	29912	54	8 (3)	7 (3)	0.53	0.33
Q9UN81	L1RE1	40259	811	56 (30)	11 (7)	1.58	0.32
Q9BYD6	MRPL1	37113	341	27 (15)	10 (7)	0.98	0.32
P36578	RPL4	47953	219	42 (12)	14 (8)	0.82	0.32
P68363	TUBA1B	50804	181	21 (8)	10 (4)	0.37	0.32
P05141	SLC25A5	33059	155	33 (11)	12 (6)	0.95	0.32
Q9UKM9	RALY	32501	133	17 (7)	9 (4)	0.63	0.32
P22087	FBL	33877	72	14 (4)	9 (3)	0.32	0.32
P40926	MDH2	35937	60	10 (2)	8 (2)	0.19	0.32
P08865	RPSA	32947	1144	57 (34)	10 (8)	1.87	0.31
Q9NR30	DDX21	87804	706	65 (37)	23 (17)	1.24	0.31
Q12905	ILF2	43263	578	37 (29)	12 (10)	1.42	0.31
O43390	HNRNPR	71184	531	44 (28)	19 (14)	1.36	0.31
O00303	EIF3F	37654	333	22 (11)	9 (7)	0.96	0.31
Q9BYD3	MRPL4	34954	322	26 (12)	8 (4)	0.89	0.31
P62753	RPS6	28834	528	44 (22)	10 (6)	1.67	0.3
Q9H0A0	NAT10	116569	289	43 (14)	28 (13)	0.56	0.3
Q96PU8	QKI	37761	194	16 (9)	8 (6)	0.66	0.3
P38919	EIF4A3	47126	95	18 (5)	14 (4)	0.5	0.3
P11142	HSPA8	71082	534	46 (24)	18 (11)	1.06	0.29
Q9HC16	APOBEC3G	47233	337	48 (24)	12 (10)	1.75	0.29
O60506	SYNCRIP	69788	971	55 (37)	17 (12)	1.18	0.28
Q92900	UPF1	125578	669	50 (31)	27 (19)	0.9	0.28
P17844	DDX5	69618	441	30 (20)	18 (10)	0.74	0.28
P02538	KRT6A	60293	187	29 (14)	16 (8)	0.61	0.28
Q13347	EIF3I	36878	104	10 (5)	8 (4)	0.41	0.28
P35250	RFC2	39588	95	12 (4)	8 (3)	0.27	0.28
Q5T653	MRPL2	33565	87	13 (4)	7 (3)	0.33	0.28
Q00839	HNRNPU	91269	2289	134 (79)	24 (16)	1.78	0.27
Q12906	ILF3	95678	511	61 (29)	21 (13)	0.6	0.27
P38159	RBMX	42306	490	36 (20)	11 (6)	0.83	0.27
P10809	HSPD1	61187	259	19 (9)	12 (8)	0.52	0.27
O75127	PTCD1	79433	258	26 (12)	15 (9)	0.62	0.27
Q15365	PCBP1	37987	153	17 (6)	7 (3)	0.4	0.27
Q96PM9	ZNF385A	40771	129	12 (4)	9 (4)	0.48	0.27
P39023	RPL3	46365	604	40 (26)	14 (13)	2.22	0.26
P04406	GAPDH	36201	148	14 (5)	8 (4)	0.42	0.26
P16401	HIST1H1B	22566	129	9 (5)	6 (4)	0.74	0.26
Q6PK04	CCDC137	33268	35	7 (1)	6 (1)	0.1	0.26
Q99729	HNRNPAB	36316	456	30 (18)	9 (4)	1.01	0.25

P52272	HNRNPM	77749	315	29 (16)	17 (9)	0.58	0.25
P16989	YBX3	40066	285	19 (9)	9 (5)	0.74	0.25
P07437	TUBB	50095	219	25 (9)	10 (5)	0.47	0.25
Q9Y262	EIF3L	66912	197	16 (6)	13 (5)	0.4	0.25
P68371	TUBB4B	50255	184	19 (8)	10 (4)	0.37	0.25
P60228	EIF3E	52587	179	17 (7)	11 (5)	0.53	0.25
O75569	PRKRA	34839	94	13 (7)	6 (3)	0.44	0.25
Q96E29	MTERF3	48055	81	93 (5)	11 (3)	0.39	0.25
Q96AG4	LRRC59	35308	74	13 (5)	7 (3)	0.57	0.25
Q08211	DHX9	142181	970	61 (38)	26 (18)	0.76	0.24
Q9BQG0	MYBBP1A	149731	467	59 (19)	31 (13)	0.41	0.24
P04259	KRT6B	60315	457	39 (26)	14 (8)	0.61	0.24
Q9BUJ2	HNRNPUL1	96250	316	30 (17)	17 (8)	0.54	0.24
P46087	NOP2	89589	315	22 (13)	15 (11)	0.54	0.24
P61978	HNRNPK	51230	211	13 (6)	10 (5)	0.45	0.24
Q13151	HNRNPA0	30993	147	17 (6)	6 (2)	0.36	0.24
Q02978	SLC25A11	34211	101	11 (2)	7 (2)	0.32	0.24
Q14498	RBM39	59628	371	21 (11)	10 (5)	0.31	0.23
Q15366	PCBP2	38955	252	17 (9)	6 (4)	0.5	0.23
P43243	MATR3	95078	248	38 (13)	17 (10)	0.78	0.23
Q9BQ39	DDX50	83084	238	28 (13)	14 (9)	0.42	0.23
P51991	HNRNPA3	39799	172	17 (4)	7 (3)	0.27	0.23
P49748	ACADVL	70745	156	16 (6)	12 (5)	0.31	0.23
P50914	RPL14	23531	152	10 (6)	5 (2)	0.49	0.23
Q96DH6	MSI2	35345	152	15 (6)	7 (4)	0.57	0.23
Q96SI9	STRBP	74290	108	22 (7)	13 (3)	0.14	0.23
Q9Y3Y2	CHTOP	26380	82	8 (1)	5 (1)	0.13	0.23
O75616	ERAL1	48833	74	10 (4)	7 (3)	0.22	0.23
Q99848	EBNA1BP2	34887	43	9 (2)	6 (2)	0.2	0.23
Q8IUX4	APOBEC3F	45846	432	33 (17)	10 (7)	0.87	0.22
Q71RC2	LARP4	81230	101	18 (4)	12 (4)	0.22	0.22
Q9BQ75	CMSS1	32149	89	18 (7)	7 (4)	0.63	0.22
Q9NUD5	ZCCHC3	44389	45	10 (1)	9 (1)	0.07	0.22
P09001	MRPL3	38893	287	15 (10)	7 (6)	0.92	0.21
Q16629	SRSF7	27578	97	10 (3)	6 (3)	0.41	0.21
Q9NX20	MRPL16	28488	74	21 (5)	6 (3)	0.94	0.21
Q14103	HNRNPD	38581	602	36 (22)	8 (4)	0.51	0.2
P11021	HSPA5	72402	335	17 (10)	12 (6)	0.36	0.2
Q96I24	FUBP3	61944	134	8 (4)	8 (4)	0.3	0.2
Q9BYG3	NIFK	34372	126	6 (3)	4 (3)	0.45	0.2
A0A0A0MS14	IGHV1-45	13614	90	3 (2)	2 (1)	0.25	0.2
Q9BRJ2	MRPL45	35613	81	18 (3)	8 (2)	0.31	0.2
O95793	STAU1	63428	71	10 (2)	9 (2)	0.16	0.2
Q7Z7H8	MRPL10	29492	65	9 (3)	4 (2)	0.24	0.2
P11387	TOP1	91125	51	28 (2)	15 (2)	0.11	0.2
Q5RKV6	EXOSC6	28503	37	7 (1)	5 (1)	0.12	0.2
P40937	RFC5	38757	34	9 (2)	7 (2)	0.18	0.2
P38646	HSPA9	73920	183	17 (7)	10 (5)	0.24	0.19
Q9UJS0	SLC25A13	74528	177	13 (6)	9 (4)	0.3	0.19

Q9BVP2	GNL3	62468	169	14 (9)	10 (7)	0.51	0.19
P55884	EIF3B	92823	157	16 (6)	13 (5)	0.19	0.19
Q9NVP1	DDX18	75702	154	19 (6)	11 (5)	0.24	0.19
Q9Y2P8	RCL1	41273	81	9 (3)	6 (3)	0.26	0.19
P62750	RPL23A	17684	63	3 (1)	2 (1)	0.19	0.19
Q9UKD2	MRTO4	27657	44	4 (1)	4 (1)	0.12	0.19
P62258	YWHAE	29326	44	5 (2)	5 (2)	0.38	0.19
Q8WVM0	TFB1M	39860	42	7 (3)	5 (2)	0.17	0.19
Q92522	H1FX	22474	358	24 (19)	6 (5)	1.31	0.18
P62917	RPL8	28235	291	24 (12)	5 (4)	1.44	0.18
P12956	XRCC6	70084	279	21 (9)	10 (6)	0.51	0.18
Q9H2U1	DHX36	115600	267	23 (12)	14 (10)	0.36	0.18
Q9H0D6	XRN2	109426	249	21 (11)	14 (7)	0.27	0.18
Q9H2W6	MRPL46	31799	202	10 (7)	5 (5)	0.82	0.18
P08238	HSP90AB1	83554	196	16 (7)	11 (4)	0.17	0.18
P35249	RFC4	40170	186	14 (7)	7 (5)	0.49	0.18
O00411	POLRMT	140300	135	25 (8)	16 (7)	0.17	0.18
Q7L2H7	EIF3M	42932	78	11 (2)	8 (2)	0.25	0.18
Q9Y2R4	DDX52	67798	57	16 (2)	9 (2)	0.1	0.18
Q9BVI4	NOC4L	58830	54	18 (2)	9 (2)	0.18	0.18
Q8WXX5	DNAJC9	30062	46	6 (1)	5 (1)	0.23	0.18
Q9BZE4	GTPBP4	74317	44	15 (2)	10 (2)	0.09	0.18
Q07352	ZFP36L1	36747	36	5 (1)	5 (1)	0.09	0.18
Q8NEJ9	NGDN	35872	32	6 (1)	4 (1)	0.09	0.18
P04792	HSPB1	22826	32	3 (1)	3 (1)	0.15	0.18
Q14152	EIF3A	166867	364	35 (17)	22 (10)	0.29	0.17
B5ME19	EIF3CL	106091	221	17 (8)	13 (7)	0.28	0.17
P07900	HSP90AA1	85006	203	18 (8)	12 (5)	0.21	0.17
P57721	PCBP3	39725	186	16 (7)	5 (3)	0.38	0.17
P35251	RFC1	128688	176	29 (5)	14 (5)	0.13	0.17
P04843	RPN1	68641	162	10 (5)	9 (5)	0.32	0.17
P19338	NCL	76625	140	28 (7)	11 (6)	0.29	0.17
Q9H936	SLC25A22	34904	85	7 (2)	5 (2)	0.2	0.17
Q9UH17	APOBEC3B	46749	82	16 (5)	7 (3)	0.31	0.17
Q15024	EXOSC7	32428	27	3 (1)	3 (1)	0.1	0.17
Q96H79	ZC3HAV1L	33967	25	3 (0)	3 (0)	0.1	0.17
O75323	NIPSNAP2	33949	16	5 (0)	5 (0)	0.1	0.17
A0A075B6S2	IGKV2D-29	13249	1706	40 (35)	2 (2)	0.58	0.16
Q7Z2W4	ZC3HAV1	103135	133	13 (4)	11 (3)	0.1	0.16
P40938	RFC3	41328	92	8 (4)	6 (3)	0.36	0.16
P52597	HNRNPF	45985	83	16 (3)	5 (2)	0.23	0.16
O00566	MPHOSPH10	78930	69	9 (3)	8 (3)	0.13	0.16
P09651	HNRNPA1	38837	62	15 (2)	6 (2)	0.18	0.16
P26368	U2AF2	53809	59	10 (2)	5 (2)	0.13	0.16
Q9NX58	LYAR	44044	52	10 (2)	5 (2)	0.24	0.16
O60762	DPM1	29673	42	5 (1)	4 (1)	0.11	0.16
P11388	TOP2A	175017	262	46 (12)	23 (9)	0.25	0.15
Q96GQ7	DDX27	90292	202	13 (7)	12 (6)	0.28	0.15
O43143	DHX15	91673	167	16 (6)	11 (4)	0.19	0.15

Q96PK6	RBM14	69620	152	12 (4)	9 (4)	0.26	0.15
P0DMV8	HSPA1A	70294	85	16 (5)	11 (5)	0.26	0.15
P50416	CPT1A	88995	77	16 (4)	11 (4)	0.2	0.15
Q13868	EXOSC2	32996	67	3 (1)	3 (1)	0.1	0.15
O75821	EIF3G	35874	65	9 (2)	5 (2)	0.19	0.15
Q00577	PURA	35003	64	13 (2)	7 (1)	0.2	0.15
Q13243	SRSF5	31359	64	8 (2)	5 (2)	0.22	0.15
P02786	TFRC	85274	61	21 (3)	9 (3)	0.12	0.15
O95831	AIFM1	67144	57	7 (1)	7 (1)	0.05	0.15
Q9BRZ2	TRIM56	83147	43	9 (1)	7 (1)	0.04	0.15
Q9NW13	RBM28	86198	41	13 (2)	9 (2)	0.08	0.15
P05023	ATP1A1	114135	219	22 (7)	11 (6)	0.18	0.14
Q5VTE0	EEF1A1P5	50495	208	19 (9)	7 (3)	0.37	0.14
P78316	NOP14	98292	154	14 (4)	10 (4)	0.14	0.14
Q15758	SLC1A5	57018	143	10 (3)	7 (3)	0.25	0.14
Q8TDD1	DDX54	98819	121	11 (3)	9 (2)	0.14	0.14
P47914	RPL29	17798	111	7 (3)	2 (1)	0.42	0.14
Q96QR8	PURB	33392	64	12 (1)	7 (1)	0.21	0.14
P60842	EIF4A1	46353	60	6 (4)	5 (3)	0.23	0.14
Q01844	EWSR1	68721	59	9 (3)	6 (2)	0.1	0.14
Q9Y5B9	SUPT16H	120409	46	19 (1)	12 (1)	0.03	0.14
P26038	MSN	67892	36	9 (1)	8 (1)	0.05	0.14
P39656	DDOST	50940	35	5 (1)	5 (1)	0.06	0.14
P02768	ALB	71317	814	40 (24)	9 (2)	0.14	0.13
P06748	NPM1	32726	334	23 (10)	4 (1)	0.21	0.13
Q2NL82	TSR1	92151	154	13 (5)	10 (4)	0.23	0.13
Q07020	RPL18	21735	85	4 (1)	2 (1)	0.15	0.13
Q9Y4P3	TBL2	50393	85	4 (2)	4 (2)	0.14	0.13
Q13601	KRR1	43866	75	7 (3)	5 (3)	0.24	0.13
P55084	HADHB	51547	69	10 (3)	7 (3)	0.2	0.13
O95218	ZRANB2	37838	63	5 (2)	4 (1)	0.09	0.13
Q8NHQ9	DDX55	69073	61	7 (1)	7 (1)	0.05	0.13
Q99623	PHB2	33276	41	5 (1)	4 (1)	0.1	0.13
P83731	RPL24	17882	38	2 (1)	2 (1)	0.19	0.13
P10155	TROVE2	61372	37	7 (1)	6 (1)	0.05	0.13
O75934	BCAS2	26229	33	4 (1)	4 (1)	0.13	0.13
Q9UG63	ABCF2	71815	29	10 (1)	7 (1)	0.05	0.13
P12004	PCNA	29092	25	3 (0)	3 (0)	0.11	0.13
P35637	FUS	53622	186	11 (8)	5 (5)	0.52	0.12
P42704	LRPPRC	159003	117	17 (6)	14 (4)	0.13	0.12
Q6P158	DHX57	157103	108	16 (3)	13 (2)	0.11	0.12
P40939	HADHA	83688	105	9 (4)	7 (4)	0.17	0.12
Q4G0J3	LARP7	67143	100	9 (4)	6 (2)	0.1	0.12
Q92804	TAF15	62021	89	8 (4)	4 (3)	0.17	0.12
P27348	YWHAQ	28032	83	3 (1)	3 (1)	0.25	0.12
O15371	EIF3D	64560	69	10 (2)	7 (2)	0.1	0.12
Q9BXP5	SRRT	101060	65	8 (1)	8 (1)	0.03	0.12
Q15293	RCN1	38866	65	5 (2)	4 (2)	0.18	0.12
P38117	ETFB	28054	63	3 (2)	3 (2)	0.4	0.12

Q99575	POP1	116346	50	15 (2)	11 (2)	0.12	0.12
O00159	MYO1C	122461	49	12 (2)	10 (2)	0.05	0.12
Q9BVJ6	UTP14A	88095	48	14 (1)	9 (1)	0.04	0.12
P14866	HNRNPL	64720	44	7 (2)	6 (2)	0.1	0.12
Q9UHB7	AFF4	127781	38	18 (1)	12 (1)	0.03	0.12
Q9UHB9	SRP68	71199	37	8 (1)	7 (1)	0.05	0.12
Q01650	SLC7A5	55659	32	6 (1)	5 (1)	0.06	0.12
P07477	PRSS1	27111	277	24 (12)	2 (1)	0.26	0.11
Q14692	BMS1	146571	188	15 (10)	12 (8)	0.25	0.11
Q9P2E9	RRBP1	152780	121	23 (2)	14 (1)	0.04	0.11
Q13428	TCOF1	152243	96	30 (1)	11 (1)	0.02	0.11
Q99459	CDC5L	92422	92	13 (3)	8 (2)	0.07	0.11
Q7Z417	NUFIP2	76132	88	10 (2)	6 (2)	0.09	0.11
Q01130	SRSF2	25461	87	6 (2)	2 (1)	0.13	0.11
O00571	DDX3X	73597	73	8 (3)	7 (2)	0.14	0.11
Q9H6S0	YTHDC2	161573	60	14 (3)	14 (3)	0.06	0.11
E9PAV3	NACA	205979	58	19 (2)	15 (2)	0.03	0.11
P13010	XRCC5	83222	57	9 (2)	8 (1)	0.08	0.11
Q9H9B4	SFXN1	35881	54	4 (2)	4 (2)	0.19	0.11
Q13283	G3BP1	52189	53	4 (1)	4 (1)	0.06	0.11
Q9H7E9	C8orf33	25319	50	2 (1)	2 (1)	0.13	0.11
P17858	PFKL	85762	49	7 (1)	7 (1)	0.04	0.11
Q9Y446	PKP3	87485	48	11 (2)	8 (2)	0.08	0.11
Q9BQA1	WDR77	37442	45	5 (2)	4 (2)	0.18	0.11
P31689	DNAJA1	45581	29	5 (1)	4 (1)	0.07	0.11
P55265	ADAR	137178	27	16 (1)	12 (1)	0.05	0.11
P61313	RPL15	24245	19	3 (0)	2 (0)	0.14	0.11
P07195	LDHB	36900	87	3 (1)	3 (1)	0.19	0.1
O75165	DNAJC13	256533	72	19 (3)	18 (3)	0.05	0.1
P05362	ICAM1	58587	71	4 (2)	4 (2)	0.12	0.1
Q13247	SRSF6	39677	71	5 (2)	4 (2)	0.17	0.1
Q13206	DDX10	101168	70	7 (2)	6 (2)	0.07	0.1
P78362	SRPK2	78219	63	9 (3)	5 (2)	0.09	0.1
A0A0C4DH68	IGKV2-24	13185	63	3 (1)	1 (1)	0.26	0.1
Q86V81	ALYREF	26872	60	4 (2)	3 (1)	0.12	0.1
P48651	PTDSS1	56175	53	6 (1)	4 (1)	0.06	0.1
Q9BRU9	UTP23	28783	52	2 (1)	2 (1)	0.12	0.1
Q8NC60	NOA1	78979	49	7 (1)	5 (1)	0.04	0.1
Q8N5C6	SRBD1	112960	49	11 (2)	10 (2)	0.06	0.1
Q9Y5J1	UTP18	62421	48	5 (1)	4 (1)	0.05	0.1
P35579	MYH9	227646	44	25 (2)	16 (2)	0.03	0.1
Q9NZ01	TECR	36410	39	4 (1)	3 (1)	0.09	0.1
P32322	PYCR1	33568	37	2 (1)	2 (1)	0.1	0.1
Q96QD9	FYTTD1	35853	37	4 (1)	4 (1)	0.09	0.1
O00299	CLIC1	27248	36	2 (1)	2 (1)	0.12	0.1
Q9Y2X3	NOP58	60054	36	5 (1)	4 (1)	0.11	0.1
Q5VWQ0	RSBN1	90928	32	6 (1)	6 (1)	0.04	0.1
P07305	H1F0	20850	29	3 (1)	2 (1)	0.16	0.1
Q15633	TARBP2	39642	29	3 (1)	3 (1)	0.08	0.1

P48634	PRRC2A	229180	29	20 (1)	15 (1)	0.01	0.1
Q9NQZ2	UTP3	54639	24	5 (1)	4 (1)	0.06	0.1
Q02880	TOP2B	184122	132	26 (5)	14 (5)	0.11	0.09
Q09161	NCBP1	92864	117	7 (4)	6 (3)	0.11	0.09
Q13200	PSMD2	100877	112	8 (4)	6 (4)	0.14	0.09
P09874	PARP1	113811	94	10 (3)	9 (3)	0.09	0.09
Q9UHX1	PUF60	60009	80	8 (2)	4 (1)	0.05	0.09
O75909	CCNK	64598	64	6 (3)	3 (2)	0.1	0.09
Q92499	DDX1	83349	62	7 (2)	6 (2)	0.08	0.09
Q9H8H2	DDX31	94770	56	6 (1)	6 (1)	0.03	0.09
Q14331	FRG1	29439	46	2 (1)	2 (1)	0.11	0.09
Q13823	GNL2	83831	43	5 (1)	5 (1)	0.04	0.09
Q03169	TNFAIP2	73015	39	6 (1)	5 (1)	0.04	0.09
Q3KQU3	MAP7D1	93106	36	8 (1)	7 (1)	0.04	0.09
P08579	SNRPB2	25470	36	3 (1)	2 (1)	0.13	0.09
Q8NDT2	RBM15B	97432	35	6 (1)	6 (1)	0.03	0.09
Q86VM9	ZC3H18	106544	33	19 (1)	7 (1)	0.03	0.09
P55060	CSE1L	111145	31	8 (1)	8 (1)	0.06	0.09
Q9UBP9	GULP1	34925	30	34 (2)	2 (1)	0.09	0.09
O60841	EIF5B	139198	30	11 (1)	10 (1)	0.02	0.09
P01859	IGHG2	36505	29	7 (1)	3 (1)	0.09	0.09
A0A0C4DH31	IGHV1-18	12926	26	1 (1)	1 (1)	0.27	0.09
Q96T17	MAP7D2	82371	26	5 (0)	5 (0)	0.04	0.09
Q9H6R4	NOL6	128368	25	10 (0)	9 (0)	0.03	0.09
Q8ND30	PPFIBP2	99053	21	11 (0)	6 (0)	0.03	0.09
O14744	PRMT5	73322	107	15 (2)	5 (2)	0.14	0.08
P42285	MTREX	118756	82	20 (3)	8 (3)	0.08	0.08
Q9Y383	LUC7L2	46942	76	6 (2)	3 (2)	0.15	0.08
Q13595	TRA2A	32726	69	3 (2)	2 (2)	0.21	0.08
O00325	SLC25A3	40525	63	9 (2)	4 (1)	0.08	0.08
O43242	PSMD3	61054	54	6 (1)	4 (1)	0.05	0.08
Q9GZR7	DDX24	96899	42	8 (3)	7 (2)	0.1	0.08
P26641	EEF1G	50429	41	5 (1)	4 (1)	0.07	0.08
Q86U38	NOP9	70136	38	7 (1)	5 (1)	0.05	0.08
Q15645	TRIP13	48863	37	10 (1)	4 (1)	0.07	0.08
Q86UE4	MTDH	63856	36	5 (1)	4 (1)	0.05	0.08
P21127	CDK11B	92821	35	7 (1)	7 (1)	0.04	0.08
Q9Y2E4	DIP2C	172939	35	11 (1)	10 (1)	0.02	0.08
Q13435	SF3B2	100279	34	6 (1)	6 (1)	0.03	0.08
Q15459	SF3A1	88888	32	5 (1)	4 (1)	0.04	0.08
Q13263	TRIM28	90261	31	7 (1)	5 (1)	0.04	0.08
P53985	SLC16A1	54593	30	6 (1)	4 (1)	0.06	0.08
P84098	RPL19	23565	17	1 (0)	1 (0)	0.14	0.08
P27708	CAD	245167	130	31 (3)	15 (3)	0.05	0.07
O75190	DNAJB6	36122	74	4 (1)	3 (1)	0.09	0.07
Q8TB72	PUM2	114715	72	5 (1)	5 (1)	0.06	0.07
Q9NXS2	QPCTL	43068	57	6 (1)	4 (1)	0.08	0.07
Q15029	EFTUD2	110336	54	6 (2)	6 (2)	0.06	0.07
Q53GQ0	HSD17B12	34416	46	2 (2)	2 (2)	0.2	0.07

Q9Y4C8	RBM19	107722	45	7 (1)	7 (1)	0.03	0.07
Q06265	EXOSC9	49545	44	3 (1)	3 (1)	0.07	0.07
A0FGR8	ESYT2	102807	43	7 (1)	6 (1)	0.03	0.07
P78527	PRKDC	473749	40	45 (1)	27 (1)	0.01	0.07
Q96RR1	TWNK	77619	37	4 (1)	4 (1)	0.04	0.07
O94906	PRPF6	107656	34	11 (1)	6 (1)	0.03	0.07
Q15434	RBMS2	44159	33	3 (1)	2 (1)	0.07	0.07
O76011	KRT34	50818	32	7 (1)	3 (1)	0.06	0.07
Q9NQT5	EXOSC3	30010	32	2 (1)	2 (1)	0.11	0.07
Q99755	PIP5K1A	63050	32	4 (1)	3 (1)	0.05	0.07
Q5T4F7	SFRP5	36508	26	3 (0)	2 (0)	0.09	0.07
P0DME0	SETSIP	34861	22	3 (0)	2 (0)	0.1	0.07
Q96QE5	TEFM	41992	17	4 (0)	3 (0)	0.08	0.07
Q9BRK4	LZTS2	73399	14	6 (0)	5 (0)	0.04	0.07
O43290	SART1	90371	108	6 (2)	4 (1)	0.07	0.06
Q8N9T8	KRI1	83004	96	4 (3)	3 (2)	0.12	0.06
Q6UN15	FIP1L1	66601	83	3 (1)	3 (1)	0.05	0.06
Q16769	QPCT	40965	83	5 (2)	2 (2)	0.17	0.06
Q86XZ4	SPATS2	59850	81	108 (1)	3 (1)	0.05	0.06
Q96KR1	ZFR	118079	77	8 (2)	5 (2)	0.06	0.06
Q16563	SYPL1	28889	77	3 (2)	2 (1)	0.12	0.06
Q9NY93	DDX56	62007	74	6 (1)	3 (1)	0.05	0.06
Q66PJ3	ARL6IP4	45287	68	2 (1)	2 (1)	0.07	0.06
Q99590	SCAF11	166319	54	8 (1)	8 (1)	0.02	0.06
P14678	SNRPB	24765	52	3 (2)	2 (1)	0.14	0.06
Q15427	SF3B4	44414	47	2 (1)	2 (1)	0.07	0.06
A6NLU5	VSTM2B	30393	42	3 (1)	1 (1)	0.11	0.06
P16615	ATP2A2	116336	42	9 (2)	7 (2)	0.06	0.06
O14646	CHD1	197707	38	17 (1)	8 (1)	0.02	0.06
Q6PCB5	RSBN1L	95381	36	5 (1)	4 (1)	0.03	0.06
Q6PGP7	TTC37	177485	35	14 (1)	10 (1)	0.02	0.06
Q96DI7	SNRNP40	39742	35	2 (1)	2 (1)	0.08	0.06
Q7Z739	YTHDF3	63936	32	6 (1)	3 (1)	0.05	0.06
Q9H7H0	METTL17	51272	32	3 (1)	3 (1)	0.06	0.06
Q9UNF1	MAGED2	65085	31	8 (1)	6 (1)	0.1	0.06
Q5C9Z4	NOM1	96768	31	7 (1)	5 (1)	0.03	0.06
Q8IVF7	FMNL3	118051	29	13 (1)	7 (1)	0.03	0.06
O75390	CS	51908	28	13 (1)	3 (1)	0.06	0.06
P27540	ARNT	87380	27	4 (0)	3 (0)	0.04	0.06
O00141	SGK1	49196	23	3 (0)	3 (0)	0.07	0.06
O75691	UTP20	320805	22	34 (0)	17 (0)	0.01	0.06
Q9H4Z3	PCIF1	81531	20	11 (0)	4 (0)	0.04	0.06
A7E2Y1	MYH7B	222392	20	18 (0)	11 (0)	0.01	0.06
O00567	NOP56	66408	80	10 (2)	3 (1)	0.05	0.05
Q8IY17	PNPLA6	151383	62	22 (1)	6 (1)	0.02	0.05
Q04637	EIF4G1	176124	59	8 (1)	7 (1)	0.06	0.05
Q15393	SF3B3	136575	54	8 (1)	5 (1)	0.02	0.05
Q9H0U3	MAGT1	38411	52	3 (2)	2 (1)	0.09	0.05
Q08J23	NSUN2	87214	52	4 (1)	4 (1)	0.04	0.05

Q6P4A7	SFXN4	38259	43	2 (1)	2 (1)	0.09	0.05
Q9Y5B6	PAXBP1	105195	39	6 (1)	4 (1)	0.03	0.05
Q5JTH9	RRP12	145037	34	8 (1)	7 (1)	0.02	0.05
P26599	PTBP1	57357	28	3 (1)	2 (1)	0.06	0.05
Q8WWM7	ATXN2L	113589	28	5 (1)	5 (1)	0.06	0.05
Q9H8Y5	ANKZF1	81562	27	4 (0)	4 (0)	0.04	0.05
Q01484	ANK2	435957	25	29 (0)	16 (0)	0.01	0.05
P08567	PLEK	40499	23	2 (0)	2 (0)	0.08	0.05
P39060	COL18A1	179389	59	7 (2)	5 (2)	0.04	0.04
P21333	FLNA	283301	36	12 (1)	10 (1)	0.01	0.04
Q5JSZ5	PRRC2B	243958	34	7 (1)	7 (1)	0.01	0.04
Q9UL40	ZNF346	33539	33	1 (1)	1 (1)	0.1	0.04
O75533	SF3B1	146479	33	5 (1)	4 (1)	0.02	0.04
P08195	SLC3A2	68180	33	2 (1)	2 (1)	0.05	0.04
O43837	IDH3B	42442	30	1 (1)	1 (1)	0.08	0.04
Q96CB9	NSUN4	43631	29	113 (1)	2 (1)	0.08	0.04
P04844	RPN2	69355	27	2 (1)	2 (1)	0.05	0.04
Q96PV0	SYNGAP1	149160	27	16 (1)	5 (1)	0.02	0.04
O15427	SLC16A3	50064	23	2 (0)	2 (0)	0.07	0.04
Q6NTF9	RHBDD2	39747	21	2 (1)	1 (1)	0.08	0.04
Q9ULW3	ABT1	31117	21	1 (0)	1 (0)	0.11	0.04
P46019	PHKA2	139404	19	9 (0)	5 (0)	0.02	0.04
Q14596	NBR1	108486	17	20 (0)	4 (0)	0.03	0.04
Q6IQ23	PLEKHA7	127626	17	3 (0)	3 (0)	0.03	0.04
Q9Y520	PRRC2C	317346	88	11 (5)	8 (4)	0.05	0.03
Q13724	MOGS	92032	60	7 (2)	3 (1)	0.04	0.03
P49756	RBM25	100467	54	2 (2)	2 (2)	0.07	0.03
Q8NDV7	TNRC6A	210967	40	5 (1)	5 (1)	0.02	0.03
Q00610	CLTC	193260	39	8 (1)	6 (1)	0.02	0.03
Q07666	KHDRBS1	48311	35	1 (1)	1 (1)	0.07	0.03
P61619	SEC61A1	52687	34	2 (1)	2 (1)	0.06	0.03
Q9UK32	RPS6KA6	84389	34	3 (1)	3 (1)	0.04	0.03
Q8N556	AFAP1	81530	33	14 (1)	3 (1)	0.04	0.03
P22314	UBA1	118858	31	5 (1)	4 (1)	0.03	0.03
Q9UBD9	CLCF1	25388	30	8 (1)	1 (1)	0.13	0.03
Q9UER7	DAXX	82064	25	2 (0)	2 (0)	0.04	0.03
P14618	PKM	58470	22	1 (0)	1 (0)	0.06	0.03
Q15637	SF1	68514	20	2 (0)	2 (0)	0.05	0.03
O15230	LAMA5	412023	48	21 (3)	6 (1)	0.01	0.02
P83105	HTRA4	51973	29	9 (1)	2 (1)	0.06	0.02
Q16531	DDB1	128142	27	2 (1)	2 (1)	0.03	0.02
Q96SZ4	ZSCAN10	82503	27	4 (0)	2 (0)	0.04	0.02
Q08345	DDR1	102032	22	2 (0)	2 (0)	0.03	0.02
Q5BKZ1	ZNF326	65955	19	1 (0)	1 (0)	0.05	0.02
Q8NB91	FANCB	99431	17	2 (0)	2 (0)	0.03	0.02
Q8TE68	EPS8L1	80487	36	9 (2)	2 (1)	0.04	0.01
Q96EK5	KIF1BP	72453	34	2 (1)	1 (1)	0.05	0.01

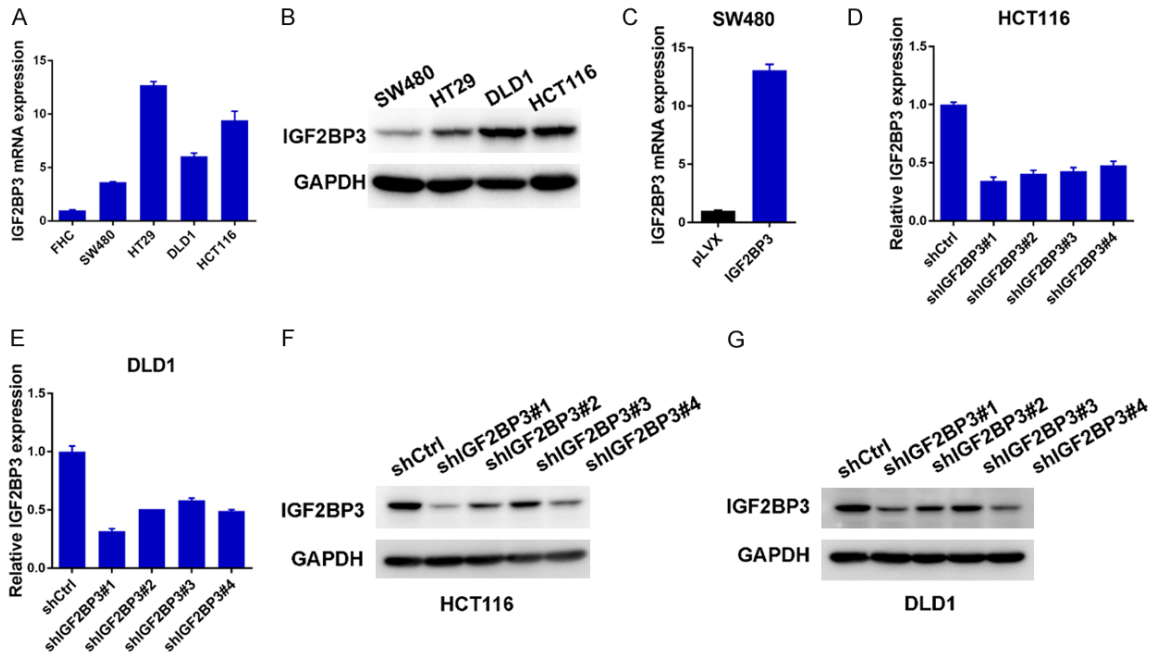

Figure S1. Analysis of IGF2BP3 expression in the indicated CRC cells. (A) RT-qPCR analysis was performed to examine the mRNA expression of *IGF2BP3* in the normal colon FHC cell line and CRC cell lines. (B) The expression of IGF2BP3 was analyzed by western blotting in CRC cells. (C) The expression of *IGF2BP3* was analyzed with RT-qPCR in the stable IGF2BP3-overexpressing SW480 cells and the control cells. (D, E) RT-qPCR analysis was performed to examine the mRNA expression of *IGF2BP3* in the HCT116 (D) and DLD1 (E) cells with stable IGF2BP3 depletion. (F, G) Western blotting was performed to analyze the expression of IGF2BP3 in the HCT116 (F) or DLD1 (G) cells with stable IGF2BP3 depletion.

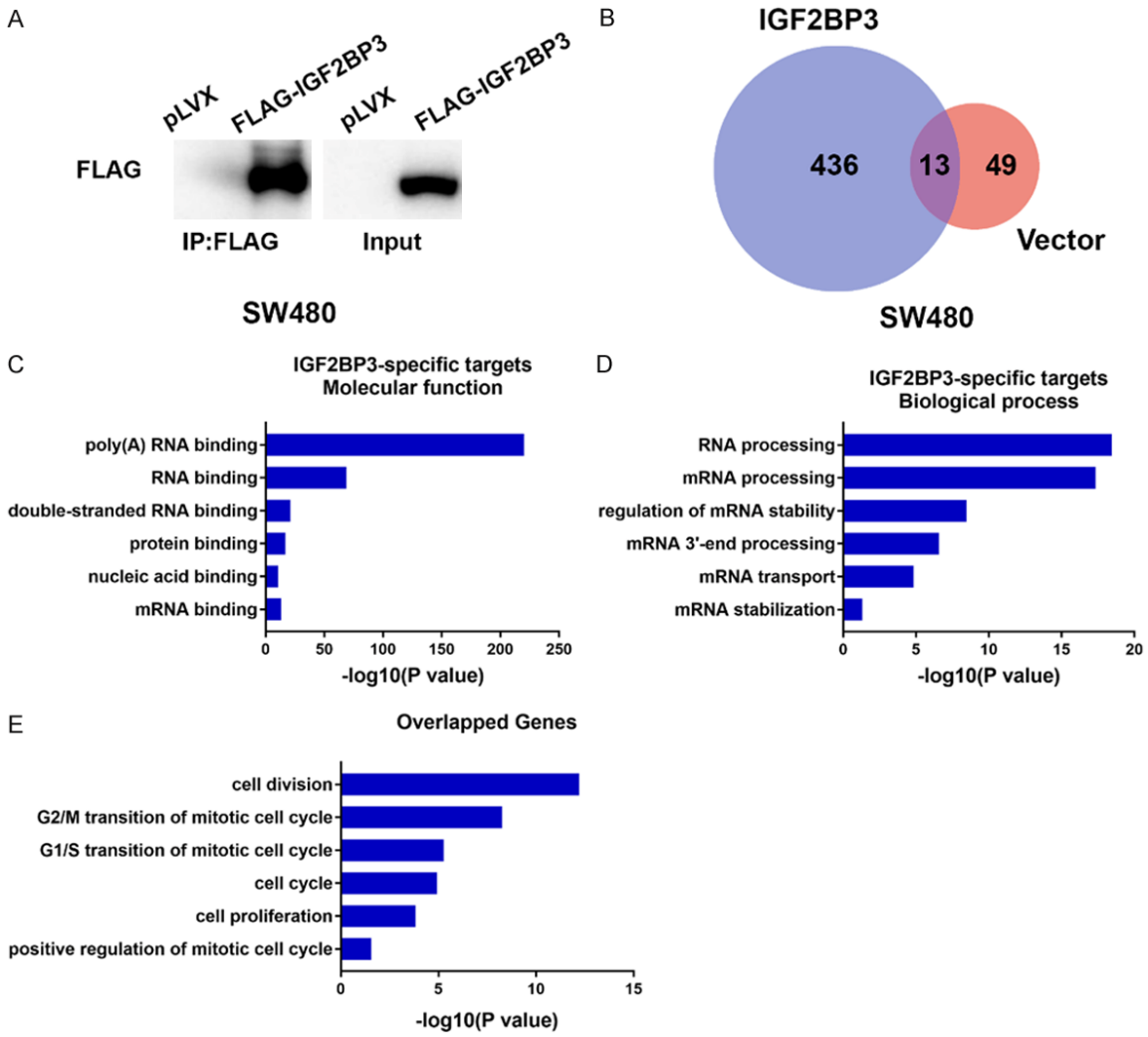

Figure S2. Bioinformatics analysis of IGF2BP3-interacted proteins and co-regulated mRNAs. (A) Whole-cell lysates from the stable FLAG-IGF2BP3-overexpressing SW480 cells and control cells were subjected to co-IP analysis with an anti-FLAG M2 affinity gel. The immunoprecipitates were then blotted using antibodies against the indicated proteins. (B) Venn diagram analysis of the interacting proteins in the FLAG-IGF2BP3-overexpressing SW480 cells and control cells according to mass spectrum assay. (C, D) GO analysis of the IGF2BP3-specific interacting proteins in SW480 cells. (E) GO analysis of the overlapping genes that were coregulated by IGF2BP3 and ELAVL1.

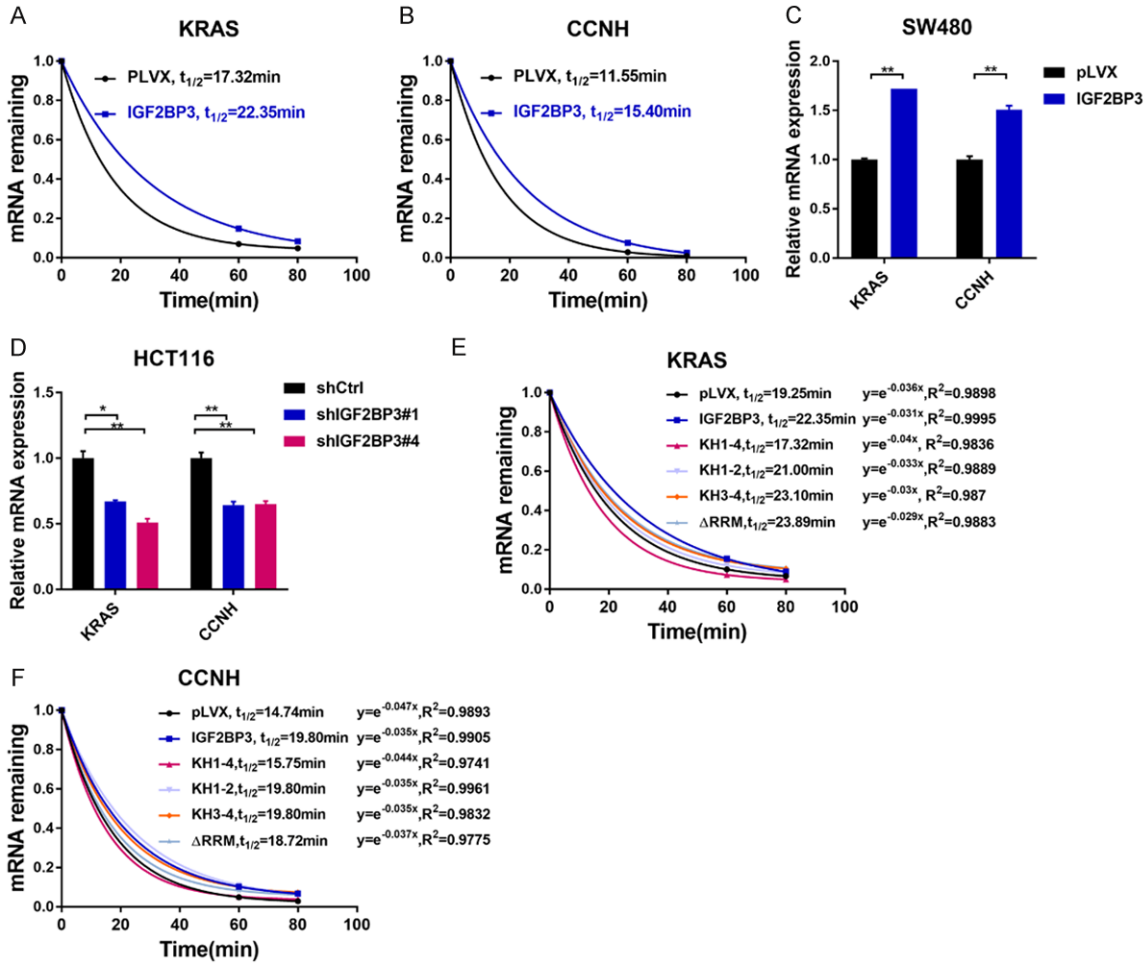

Figure S3. Regulation of mRNA stability by IGF2BP3. (A, B) Both the IGF2BP3-overexpressing SW480 cells and control cells were treated with actinomycin D for 60 and 80 min respectively. Total RNA was extracted, the relative expression of *KRAS* (A) and *CCNH* (B) was calculated, and the mRNA half-lives of these genes were analyzed. (C) The mRNA expression of *KRAS* and *CCNH* was analyzed in the IGF2BP3-overexpressing SW480 cells and control cells. (D) The mRNA expression of *KRAS* and *CCNH* was analyzed in the IGF2BP3-deficient HCT116 cells and control cells. (E, F) The indicated IGF2BP3 deletion mutants and IGF2BP3 (WT) were stably overexpressed in SW480 cells. Cells were treated with actinomycin D for 60 and 80 min respectively. Total RNA was extracted, the relative expression of *KRAS* (E) and *CCNH* (F) was calculated, and the mRNA half-lives of these genes were analyzed. **P<0.05*, ***P<0.01*.

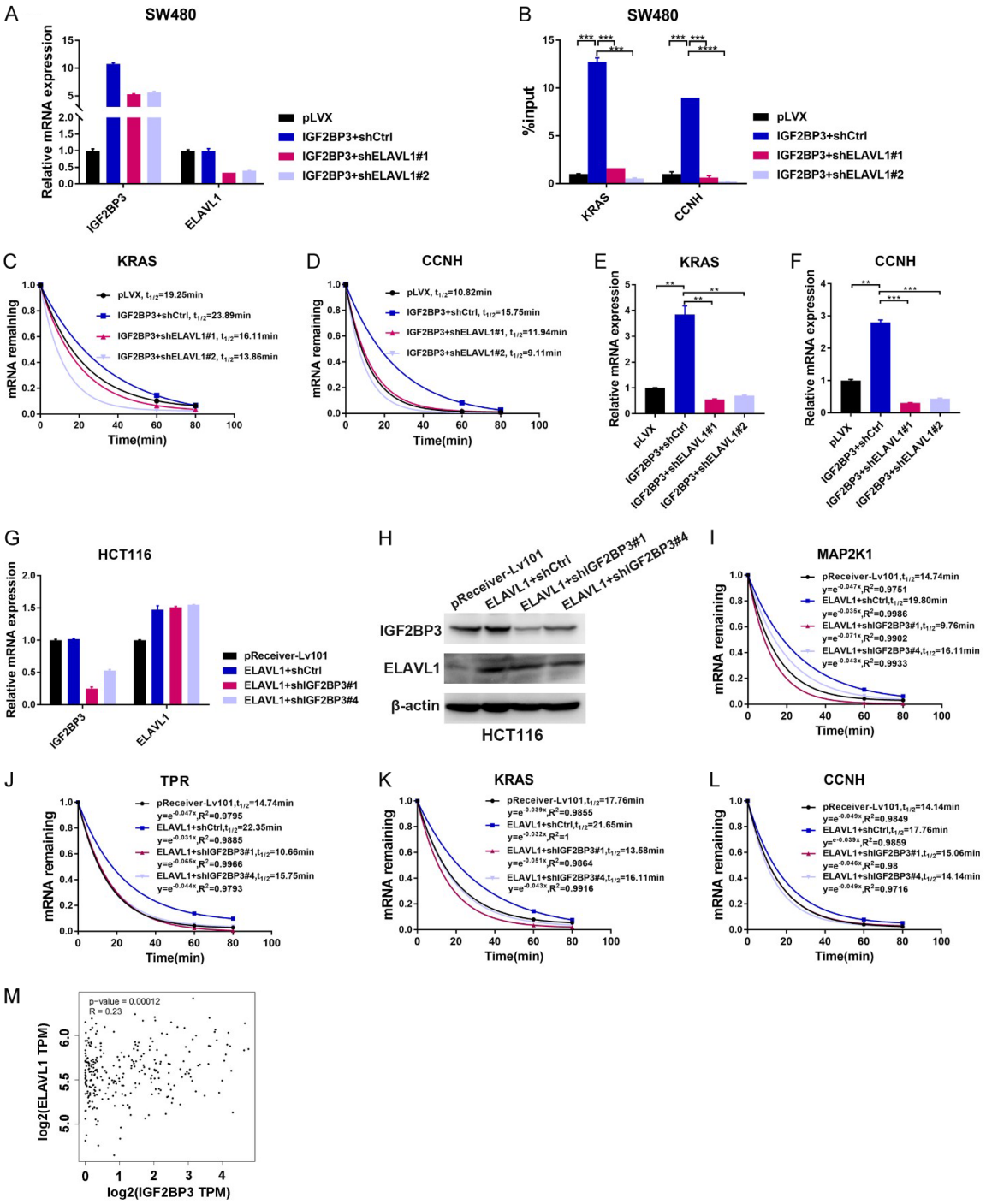

Figure S4. IGF2BP3 cooperates with ELAVL1 to regulate mRNA stability. (A) The expression of ELAVL1 was depleted in IGF2BP3-overexpressing SW480 cells. RT-qPCR analysis was performed to detect the expression of *IGF2BP3* and *ELAVL1*. (B) RIP analysis was performed to analyze the IGF2BP3 binding to the regulatory regions of the *KRAS* and *CCNH* mRNA in the SW480 cells overexpressing IGF2BP3 and these cells with the additional stable depletion of ELAVL1. (C, D) Both the IGF2BP3-overexpressing SW480 cells and these cells with the additional stable depletion of ELAVL1 were treated with actinomycin D for 60 and 80 min respectively. Total RNAs were extracted, the relative expression of *KRAS* (C) and *CCNH* (D) was calculated, and the mRNA half-lives of these genes were analyzed. (E, F) RT-qPCR assay was performed to evaluate the mRNA expression of *KRAS* (E), and *CCNH* (F) in the IGF2BP3-overexpressing SW480 cells and these cells with the additional stable ELAVL1 depletion. (G) The expression of IGF2BP3 was depleted in ELAVL1-overexpressing HCT116 cells. RT-qPCR analysis was performed to detect the expression of *IGF2BP3* and *ELAVL1*. (H) Western blot analysis was performed to detect the expression of IGF2BP3 and ELAVL1

in ELAVL1-overexpressing HCT116 cells and these cells with additional stable depletion of IGF2BP3. (I-L) Both the ELAVL1-overexpressing HCT116 cells and these cells with additional stable depletion of IGF2BP3 were treated with actinomycin D for 60 and 80 min respectively. Total RNA was extracted, and the mRNA half-lives of *MAP2K1* (I), *TPR* (J), *KRAS* (K), *CCNH* (L) were analyzed. (M) Analysis of the clinical correlations between *IGF2BP3* and *ELAVL1* expression with the GEPIA database [1]. *P<0.05, **P<0.01, ***P<0.001, ****P<0.0001.

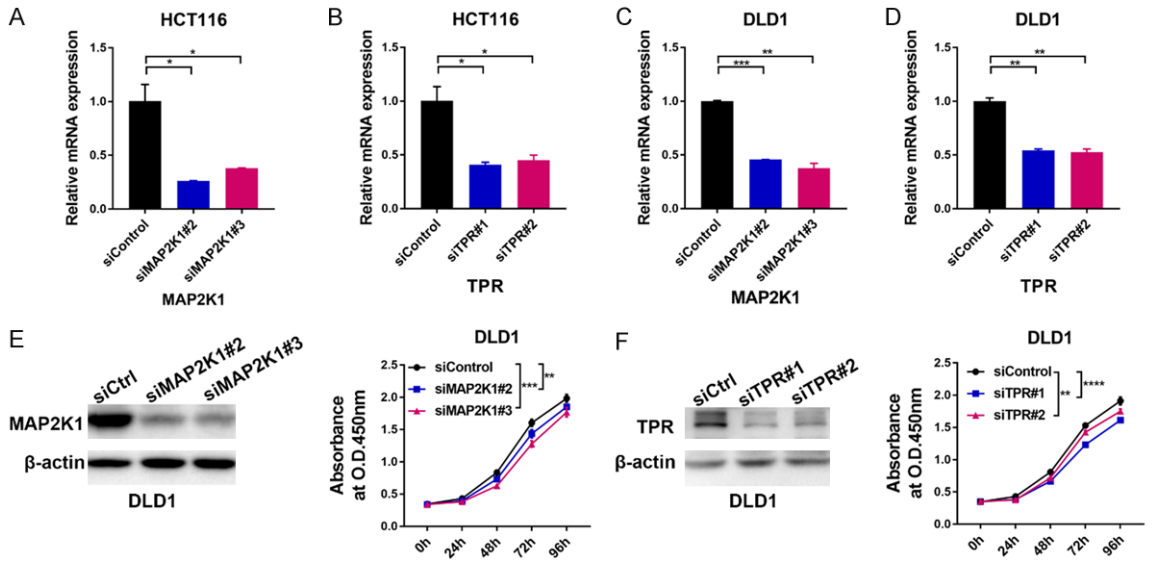

Figure S5. Knockdown of MAP2K1 or TPR suppresses the proliferation of DLD1 cells. (A, B) The mRNA expression of *MAP2K1* and *TPR* was analyzed in the HCT116 cells transfected with siRNA targeting *MAP2K1* (A) or *TPR* (B) and nontargeting control siRNA. (C, D) The mRNA expression of *MAP2K1* and *TPR* was analyzed in the DLD1 cells transfected with siRNA targeting *MAP2K1* (C) or *TPR* (D) and nontargeting control siRNA. (E, F) DLD1 cells were transfected with siRNA targeting *MAP2K1* or *TPR* and nontargeting siRNA control, and the knockdown efficiency of MAP2K1 (E, left panel) and TPR (F, left panel) was confirmed with western blotting analysis. The effect of *MAP2K1* and *TPR* silencing on the proliferation of DLD1 cells was analyzed with a CCK-8 assay (E, F right panel). **P<0.05*, ***P<0.01*, ****P<0.001*, *****P<0.0001*.

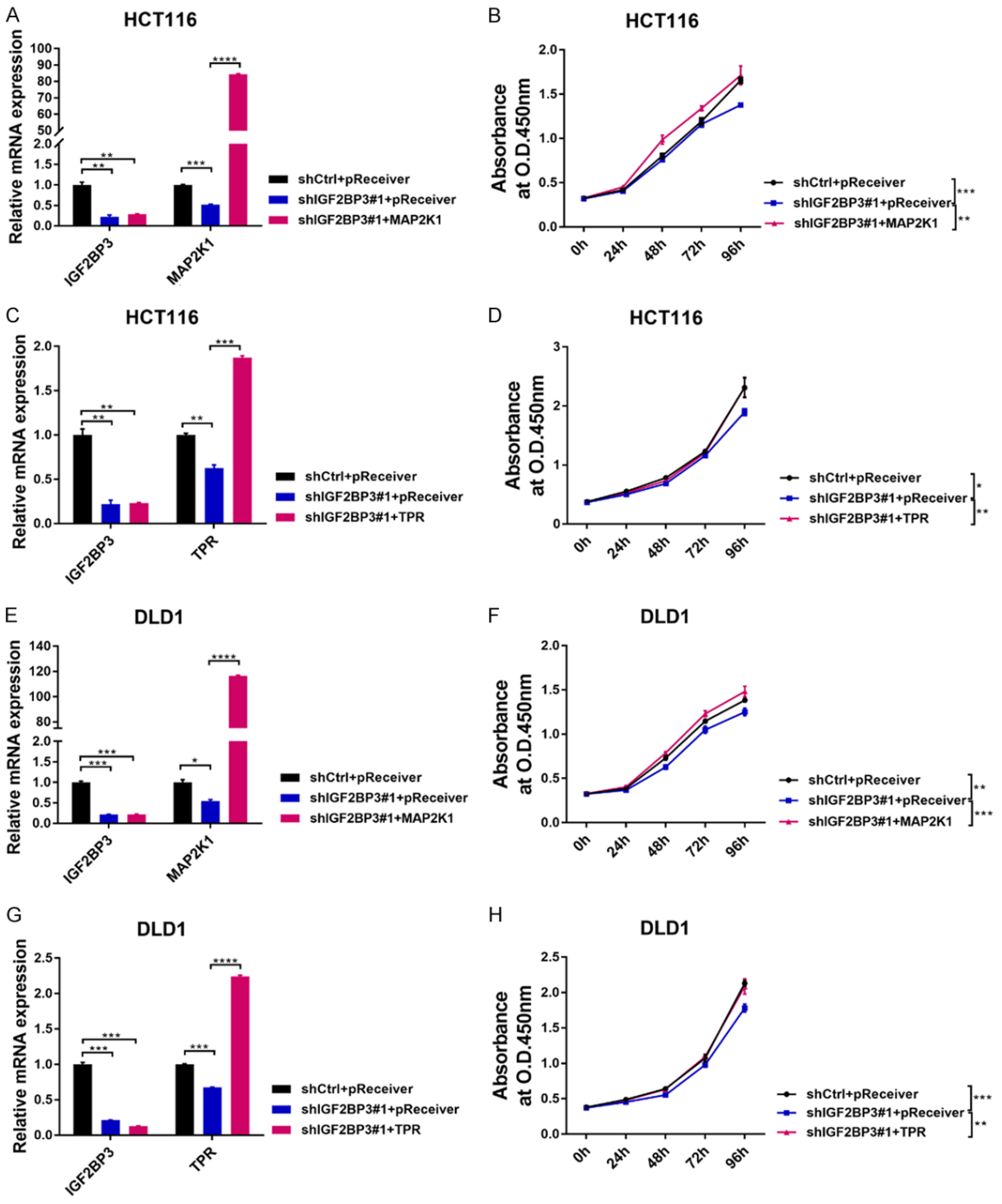

Figure S6. Ectopic expression of MAP2K1 or TPR rescues the proliferation of IGF2BP3-depleted HCT116 and DLD1 cells. (A-D) The IGF2BP3-depleted HCT116 cells were further overexpressed with MAP2K1 (A) and TPR (C). The expression of *IGF2BP3, MAP2K1* and *TPR* was analyzed with RT-qPCR analysis. The proliferation of the indicated cell was examined with a CCK-8 assay (B, D). (E-H) The IGF2BP3-depleted DLD1 cells were further overexpressed with MAP2K1 (E) and TPR (G). The expression of *IGF2BP3, MAP2K1* and *TPR* was analyzed with RT-qPCR analysis. The proliferation of the indicated cell was examined with a CCK-8 assay (F, H). *P<0.05, **P<0.01, ***P<0.001, ****P<0.0001.